

## OPEN ACCESS

## EDITED BY

Andrew James Manning,  
HR Wallingford, United Kingdom

## REVIEWED BY

Lin Mu,  
Shenzhen University, China  
Cléa Lumina Denamiel,  
Ruđer Bošković Institute, Croatia

## \*CORRESPONDENCE

Omar Knio  
✉ omar.knio@kaust.edu.sa

RECEIVED 13 March 2023

ACCEPTED 28 April 2023

PUBLISHED 27 June 2023

## CITATION

Hammoud MAER, Mittal HVR, Le Maître O,  
Hoteit I and Knio O (2023) Variance-based  
sensitivity analysis of oil spill predictions in  
the Red Sea region.  
*Front. Mar. Sci.* 10:1185106.  
doi: 10.3389/fmars.2023.1185106

## COPYRIGHT

© 2023 Hammoud, Mittal, Le Maître, Hoteit  
and Knio. This is an open-access article  
distributed under the terms of the [Creative  
Commons Attribution License \(CC BY\)](#). The  
use, distribution or reproduction in other  
forums is permitted, provided the original  
author(s) and the copyright owner(s) are  
credited and that the original publication in  
this journal is cited, in accordance with  
accepted academic practice. No use,  
distribution or reproduction is permitted  
which does not comply with these terms.

# Variance-based sensitivity analysis of oil spill predictions in the Red Sea region

Mohamad Abed El Rahman Hammoud<sup>1</sup>, H. V. R. Mittal<sup>2</sup>,  
Olivier Le Maître<sup>3</sup>, Ibrahim Hoteit<sup>1</sup> and Omar Knio<sup>2\*</sup>

<sup>1</sup>Physical Sciences and Engineering Division, King Abdullah University of Science and Technology, Thuwal, Saudi Arabia, <sup>2</sup>Computer Electrical and Mathematical Sciences and Engineering Division, King Abdullah University of Science and Technology, Thuwal, Saudi Arabia, <sup>3</sup>Centre de Mathématiques Appliquées, Centre national de la recherche scientifique (CNRS) and Inria, Ecole Polytechnique, Palaiseau, France

To support accidental spill rapid response efforts, oil spill simulations may generally need to account for uncertainties concerning the nature and properties of the spill, which compound those inherent in model parameterizations. A full detailed account of these sources of uncertainty would however require prohibitive resources needed to sample a large dimensional space. In this work, a variance-based sensitivity analysis is conducted to explore the possibility of restricting *a priori* the set of uncertain parameters, at least in the context of realistic simulations of oil spills in the Red Sea region spanning a two-week period following the oil release. The evolution of the spill is described using the simulation capabilities of Modelo Hidrodinámico, driven by high-resolution metocean fields of the Red Sea (RS) was adopted to simulate accidental oil spills in the RS. Eight spill scenarios are considered in the analysis, which are carefully selected to account for the diversity of metocean conditions in the region. Polynomial chaos expansions are employed to propagate parametric uncertainties and efficiently estimate variance-based sensitivities. Attention is focused on integral quantities characterizing the transport, deformation, evaporation and dispersion of the spill. The analysis indicates that variability in these quantities may be suitably captured by restricting the set of uncertain inputs parameters, namely the wind coefficient, interfacial tension, API gravity, and viscosity. Thus, forecast variability and confidence intervals may be reasonably estimated in the corresponding four-dimensional input space.

## KEYWORDS

Red Sea, oil spill, parametric uncertainty, regularized regression, polynomial chaos expansion, global sensitivity analysis

## 1 Introduction

Oil spill forecasting is extremely important in preventive planning and post-oil spill management. Forecasting requires a solid understanding of the prevailing oil spill dynamics, typically gained through a high-fidelity model that captures the transport of oil and its physio-chemical transformations, referred to as weathering (Zodiatis et al.,

2021). Weathering processes include evaporation, dispersion into the water column, emulsification, and spreading (Lehr et al., 2002), all of which depend on the local atmospheric and oceanic conditions (Oudot et al., 1998; Transportation Research Board and National Research Council, 2003).

Most oil spill models employ a Lagrangian particle tracking algorithm (van Sebille et al., 2018), for example, MEDSLIK II (De Dominicis et al., 2013b; De Dominicis et al., 2013a) and Modelo Hidrodinámico [MOHID; <http://www.mohid.com/>; e.g., (Neves, 2013)]. These models rely on ocean currents and atmospheric conditions and incorporate parametrizations to account for subgrid-scale processes. When subgrid parametrizations are adequately calibrated, and the spill conditions are faithfully described, the spill models effectively forecast the evolution of oil spills (Hodges et al., 2015; Barker et al., 2020).

Many sources of uncertainty arise when modeling oil spills in oceanic flows, including uncertainties in metocean conditions, forcing and model parameters (Xu et al., 2012; Iskandarani et al., 2016a; Iskandarani et al., 2016b). In a rapid response scenario, these uncertainties may be further compounded by a lack of knowledge of the nature of the spill oil and/or its physical properties. Addressing all these sources of uncertainty simultaneously is computationally prohibitive, and it is consequently advantageous to explore whether it is possible to ignore some of the uncertain inputs characterizing oil properties and model parametrizations, without significantly deteriorating our ability to quantify the variability of the predictions. This is the central question that we explore in the present study, namely in the framework of a limited, two-week long, simulations of oil spills in the RS region, which is at risk of oil spill events due to the significant number of oil tankers traversing the basin (Alkhshall and Westcott, 2019; Kleinhaus et al., 2020; Kostianaia et al., 2020; Dong et al., 2022). Our approach to this question is based on considering a limited set of scenarios that captures the diversity of met-ocean conditions in the region, and to conduct a systematic analysis of the impact of parametric uncertainties for this set of scenarios. This offers to enable us to identify *a priori* a small set of key parameters that dominate the variability of the predictions, and to ignore the others. Of course, such parameter space would lead to substantial gains, as one would be able to determine confidence bounds at a reduced computational burden.

Despite its fundamental and practical relevance, little work has been done in the literature to quantify the sensitivity of oil spill forecasts on the oil and model parameters. Previous studies dealt with a qualitative assessment of the model output's sensitivity to input parameters (Lopes, 2016), whereas others were relied on a quantitative assessment based on local sensitivities (Mateus and Franz, 2015); namely on relative model output variation for variations in the input, or based on a normalized error approach (Oliveira et al., 2020). Whereas local sensitivity methods provide simple and effective means to analyze forecast variability, their application to reduce the space of random parameters may be prone to errors, especially when mixed effects are important. To overcome such potential drawbacks, global sensitivity analysis (GSA) considers the full space of uncertain inputs (Adetula and Bokov, 2011). Generally, GSA implementations are categorized as variance-

based (Sobol, 1993; Homma and Saltelli, 1996; Sobol, 2001) or entropy-based (Lüdtke et al., 2008; Martorell et al., 2008). In both cases, the analysis considers the variability of an entire set of parameters, simultaneously and in the entire range of their priors (Sudret, 2008). Additionally, it yields total sensitivity indices that account for both direct and mixed interactions, providing robust means for identifying which parameters can be effectively neglected.

In the present study, we rely on Sobol's total sensitivity indices to analyze the variability of the model forecast (Homma and Saltelli, 1996). These provide a variance-based estimate of the sensitivity of selected model outputs due to uncertainties in individual parameters. This approach relies on an orthogonal hierarchical decomposition of the variance to produce robust estimates that can be readily leveraged for the purpose of parameter space reduction. It has in fact shown to be an effective tool in a different areas, including ocean modeling applications (Srinivasan et al., 2010; Alexanderian et al., 2012; Winokur et al., 2013; Goncalves et al., 2016; Wang et al., 2016) among others [e.g. (Navarro Jimenez et al., 2016; Huan et al., 2018; KC et al., 2021)].

The paper is structured as follows. Section 2 outlines the scope of the study, providing a brief description of the oil spill model, the selection of metocean conditions and spill scenarios, and of a screening study used to define a reasonable set of key uncertain inputs. As described in Section 3, a polynomial chaos (PC) approach is adopted to construct surrogates of selected quantities of interest (QoIs), quantify variances, and efficiently estimate Sobol indices (Crestaux et al., 2009). Simulation results are presented and analyzed in Section 4. Concluding remarks are provided in Section 5.

## 2 Data and methodology

This section describes the metocean data of the RS, which were used to drive the oil spill model. Specifically, Sections 2.1.1 and 2.1.2 describe the metocean fields and their spatial and seasonal variabilities, respectively. The selected oil spill scenarios are outlined in Section 2.1.3. Section 2.2 presents the oil spill model employed to simulate the evolution of an oil spill. The QoIs describing the evolution of the oil slick geometry, transport, and weathering processes are reported in Section 2.3. Finally, Section 2.4 discusses the screening process conducted to select uncertain parameters with the strongest influence on the released oil.

### 2.1 Red Sea and metocean dataset

#### 2.1.1 Metocean numerical modeling

The RS hosts one of the world's most diverse tropical marine habitats (Chiffings et al., 1995), including the third-largest coral reef system in the world (Carvalho et al., 2019). Fisheries, water desalination plants, and several mega-projects, such as NEOM, lie along its coast (Hoteit et al., 2021). The RS seasonally and regionally experiences widely varying metocean conditions (Yao et al., 2014a; Yao et al., 2014b). Accordingly, the RS is divided into three regions: the northern, central, and southern RS, each with unique but interweaving circulation patterns (Carvalho et al., 2019).

Further described below, the RS metocean fields we employ in the present work were extracted from high-resolution simulations (Langodan et al., 2017; Viswanadhapalli et al., 2017; Dasari et al., 2019; Hoteit et al., 2021), which provide reliable descriptions of the oceanic and atmospheric circulation of the RS region. The zonal and meridional winds were extracted from an in-house 5-km regional atmospheric reanalysis specifically generated for the RS region using the weather research forecasting (WRF) model. The WRF initial and boundary conditions were obtained from the European Centre for Medium-Range Weather Forecasts Reanalysis Interim (Dee et al., 2011) data. The WRF downscaling simulations were performed using the consecutive daily reinitialization method over 36-h periods (Viswanadhapalli et al., 2017; Dasari et al., 2019). The wave conditions in the RS were reconstructed using the WAVEWATCH III model forced with the mentioned high-resolution WRF reanalysis winds on a 1-km grid (Langodan et al., 2017).

The three-dimensional (3D) ocean currents were simulated using the Massachusetts Institute of Technology general circulation model (MITgcm) (Marshall et al., 1997) implemented at an approximately 1-km grid resolution with 50 nonuniform vertical layers. The model was forced with the mentioned WRF atmospheric reanalysis fields and open boundary in the Gulf of Aden, which were obtained from the Copernicus Marine and Environment Monitoring Service global ocean reanalysis fields, on a 6-h and 24-h basis, respectively (<https://marine.copernicus.eu/>). Readers are referred to (Hoteit et al., 2021) for a detailed description and validation of the WRF, WAVEWATCH III, and MIT general circulation model fields.

### 2.1.2 Variability of metocean condition in the Red Sea

The high mountain ranges on both sides of the RS force the wind to blow along its main axis (Langodan et al., 2014). During summer, from April to October, a northwesterly wind blows along the whole length of the sea (Langodan et al., 2014). In winter, the same northerly wind dominates over the northern part of the basin, and southeasterly winds associated with the northeasterly winds of the monsoon in the Indian Ocean prevail over the southern RS. The coexistence of northerly and southerly winds creates a convergence zone at the center of the RS (Langodan et al., 2017). The larger and smaller valleys across the bordering mountain ridge lead to typical local winds relevant for characterizing local wind regimes, for example, the wind passing through the Tokar Gap along the Sudan coast in summer and the westward blowing jets along the northeastern coast of the RS in winter (Langodan et al., 2014; Viswanadhapalli et al., 2017).

The wave variability in the RS is naturally associated with the dominant regional wind regimes (Langodan et al., 2014). During summer, the northwesterly winds prevailing over the whole RS generate mean wave heights of 1 to 1.5 m in the north (Langodan et al., 2014). In winter, the monsoon-associated winds generate mean wave heights of approximately 2 m in the southern RS, leading to a convergence zone in the central part when they meet the waves from the north (Langodan et al., 2017).

The mean surface circulation in the southern RS is largely moderated by the wind regime, which reverses between seasons. During winter, when the southeasterly winds prevail, the surface inflow from the Gulf of Aden intensifies as a western boundary current in the southern basin and switches to an eastern boundary current north of 24°N (Yao et al., 2014a). In summer, the dominant northeasterly winds push the surface outflow from the RS into the Gulf of Aden (Yao et al., 2014b). In the central and northern RS regions, circulation is primarily characterized by multiple mesoscale eddies that tend to become more energetic during winter following the development of intense baroclinic instabilities (Zhan et al., 2019), except for some strong semi-permanent wind-driven gyres that occur in summer (Zhan et al., 2019).

### 2.1.3 Oil spill scenarios

Pertaining to our main objective of exploring whether the space of uncertain parameters can be restricted *a priori*, eight scenarios were selected corresponding to four release locations and two release times. Note that the selection was guided by a desire to cover a wide range of relevant environmental conditions, particularly to build confidence in any *a priori* reduction. Of course, the surrogate models constructed for the selected metocean conditions are not expected to be representative of other ocean states. However, quantitative variability and sensitivity trends established for a sufficiently diverse set of scenarios are also expected to hold in more general conditions.

The selected release locations are depicted in Figure 1, which also displays some of the surface fields at the first of January and August. Specifically, the selected release locations include one spot in the northern RS, two in the central RS, and one in the southern RS. Spills initiated on the first of January and another on the first of August were selected to assess the influence of various metocean circulation conditions on the oil spill dynamics. As can be seen from the illustrations provided in Figure 1, the selected metocean conditions reflect distinct ocean states. Specifically, the spill conditions considered may be initiated at the center or periphery of coherent ocean eddies, or in situations characterized by turbulent small scale eddies. Similarly, the release may occur in conditions involving large or small wave heights, strong or weak surface winds, and high or low sea surface temperature. The resulting diversity of release conditions considered thus helps build confidence that any *a priori* reduction in the space of parameters that results from the analysis will also hold generally hold for the Red Sea region.

The release locations in the central RS cover the center and periphery of a long-lived eddy that experiences predictable movement during summer but more complex chaotic motion during winter. The release location in the northern RS is prone to strong wind effects that generate strong waves during summer. The circulation in the north is also dominated by mesoscale eddies that intensify in energy in winter. Finally, release Location 4 is selected to examine the influence of the metocean conditions in the south, which are tightly related to the Indian Monsoon, and the effect of the inflow current from the Arabian Sea. In the analysis below, Location 1 is the release location in the northern RS, and Location 2 is the release location at the center of the eddy in the central RS.

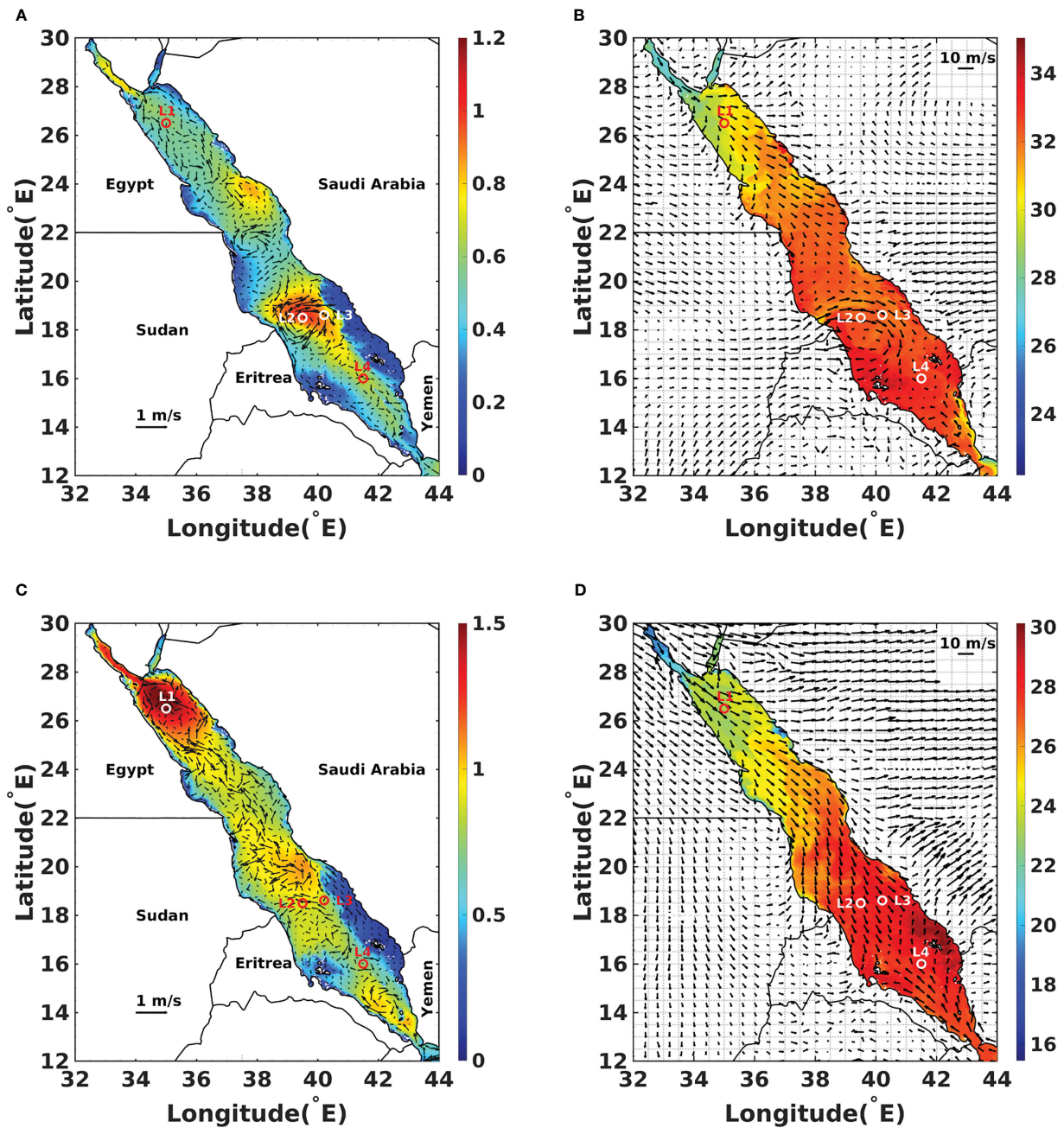


**FIGURE 1**  
 Left column (A, C): composite illustration of significant wave height (m) and surface currents (m/s); right column (B, D): composite illustration of sea surface temperature (°C) and surface winds (m/s). The top (A, B) and bottom (C, D) rows illustrate the average fields for the first of August and January of 2016, respectively. The release locations L1–4 are also depicted.

Location 3 is the release location at the periphery of the eddy in the central RS, and Location 4 is the release location in the southern RS.

## 2.2 Oil spill model

Modelo Hidrodinâmico's (MOHID) Lagrangian and oil models are components of the MOHID Water Modeling System (<http://www.mohid.com/>) adopted to simulate the results of oil spills. In addition, MOHID is an open-source, 3D water modeling system

developed by the Marine and Environmental Technology Research Center at the Technical University of Lisbon (Leitao et al., 2013). Together, the models simulate oil trajectories while accounting for the physico-chemical transformations of the oil. The Lagrangian model is responsible for transporting individual particles, accounting for the effects of diffusion, buoyancy, Stokes drift, windage, linear degradation, and land interaction, such as beaching. Moreover, the oil model simulates the effects of the weathering processes, including dispersion, evaporation, sedimentation, spread, dissolution, and emulsification. The

MOHID Lagrangian and oil spill models are driven by the outputs of the high-resolution RS metocean fields discussed in Section 2.1.1 (Hoteit et al., 2021).

A Cartesian grid uniformly spaced in the horizontal directions, longitude and latitude, and nonuniformly spaced in vertical layers was adopted for the current applications. The grid covers the entire RS between longitudes 32°E and 46°E and latitudes 10°N and 30°N up to a depth of approximately 2,746 m. The longitudinal and latitudinal axes are divided into 1,401 and 2,001 equally spaced nodes, respectively, corresponding to a grid resolution of approximately 1 km on both axes. The metocean input fields, including the daily averaged 3D ocean currents, hourly winds, wave height, and period, are specified on the same horizontal and vertical grids. The time step of the oil model was set to 60 s to properly describe the weathering processes, which vary over very short time scales, and the results were reported at 15-min intervals. The time step of the Lagrangian model to transport the individual particles was set to 3,600 s, and the results were reported at 3-h intervals. For each release scenario, 5,000 oil particles were released from the release point, where the Lagrangian and oil models advected and simulated weathering under metocean conditions. The performance and accuracy of MOHID for oil spill modeling have already been demonstrated in many previous studies and ocean basins [e.g., (Li, 2017) and (Mittal et al., 2021)].

### 2.3 Quantities of interest

This section discusses the QoIs used to characterize the transport and geometry of the oil slick and selected weathering processes. We explored several ways to characterize the shape and deformation of the surface oil. Specifically, we examined the second-order particle moments centered on the centroid of the realized oil slick or nominal oil slick. A more detailed description of these integral quantities is provided. We also investigated distance measures between the realized and reference spills, such as the Hausdorff distance and the  $\ell_2$  distance between concentration or binary maps, attributing a value of 1 to the grid cells with surface oil and 0 for no oil. For brevity, we focus on the central and nominal second-order particle moments.

The general  $(p, q)$ -moment is defined according to the following:

$$M_{p,q} = \sum_i x_{1,(i)}^p x_{2,(i)}^q, \tag{1}$$

where the sum is performed over all surface particles with nonzero mass. The transportation of the oil slick is characterized by the location of its centroid or first moment, estimated as follows:

$$\bar{x} = \frac{M_{1,0}}{M_{0,0}} = \frac{\sum_i x_{1,(i)}^1 x_{2,(i)}^0}{N}, \tag{2}$$

$$\bar{y} = \frac{M_{0,1}}{M_{0,0}} = \frac{\sum_i x_{1,(i)}^0 x_{2,(i)}^1}{N}, \tag{3}$$

where  $N$  is the total number of particles with a nonzero mass. These equations yield the longitude and latitude of the centroid (C Lon and C Lat, respectively) that describe the mean geometric location of the oil slick.

To characterize the shape of the surface slick, we rely on the second-order central particle moments (Rocha et al., 2002). Specifically, we extracted the particle covariances expressed by the following:

$$a = \frac{M_{2,0}}{M_{0,0}} - \bar{x}^2 = \frac{\sum_i x_{1,(i)}^2 x_{2,(i)}^0}{N} - \bar{x}^2, \tag{4}$$

$$b = \frac{M_{1,1}}{M_{0,0}} - \bar{x} \bar{y} = \frac{\sum_i x_{1,(i)}^1 x_{2,(i)}^1}{N} - \bar{x} \bar{y}, \tag{5}$$

$$c = \frac{M_{0,2}}{M_{0,0}} - \bar{y}^2 = \frac{\sum_i x_{1,(i)}^0 x_{2,(i)}^2}{N} - \bar{y}^2, \tag{6}$$

which enables characterizing an elliptical region associated with the surface slick.

In addition, the second-order moments relative to the nominal oil slick centroid are introduced, leading to covariances denoted by  $\hat{a}$ ,  $\hat{b}$ , and  $\hat{c}$ , which are obtained by replacing  $\bar{x}$  and  $\bar{y}$  in the system above with  $\bar{x}_o$  and  $\bar{y}_o$ , respectively, which are the longitude and latitude of the centroid of the nominal oil slick. The nominal scenario corresponds to the deterministic prediction obtained using the average value of the input parameters. Whereas  $a$ ,  $b$ , and  $c$  characterize the shape of individual oil slicks,  $\hat{a}$ ,  $\hat{b}$ , and  $\hat{c}$  characterize the region where spilled oil is likely to be present.

Finally, we rely on the fraction of mass evaporated (FME) and the fraction of mass dispersed (FMD) to characterize weathering processes. In addition, the QoIs are summarized and briefly described in Table 1. Figure S1 illustrates an example for release at Location 3 during summer. The distribution of surface oil particles and the ellipse characterized using the first and second particle moments are presented.

### 2.4 Uncertain input parameters

The evolution of simulated ocean oil spills is governed by several parameters related to the physical oil properties and model parametrizations. An initial screening was conducted by varying a single parameter at a time and observing its effects on the oil spill evolution. The parameters examined in this preliminary screening study are summarized in Table 2. These include Fay's spread, the empirical thickness gradient (ETG) spread coefficient, the emulsification coefficient, the water uptake parameter (WUP), wind coefficient (WC), the American Petroleum Institute gravity (API), pour point temperature, asphaltene content, dynamic viscosity, and interfacial tension (IFT).

The effects of each parameter in Table 2 on the QoIs were analyzed, focusing on the resulting total (peak-to-peak) variability. The results indicated that the parameters with the strongest

TABLE 1 Quantities of interest and their associated abbreviations or notation and descriptions.

Quantity of Interest	Abbreviation or Notation	Description
Fraction of Mass Dispersed	FMD	Ratio of the oil mass dispersed into the water column to the total released oil mass, which is a measure of one mode of weathering.
Fraction of Mass Evaporated	FME	Ratio of the evaporated oil mass to the total released oil mass, which is a measure of weathering by evaporation
Longitude of the Centroid	C Lon	Location of the centroid of the particles comprising the surface oil slick along the longitudinal direction.
Latitude of the Centroid	C Lat	Location of the centroid of the particles comprising the surface oil slick along the latitudinal direction.
Second-Order Central Moments	a	First diagonal entry of the particle covariance matrix. Characterizes the stretch of the ellipse fitting the oil slick along the longitudinal direction.
	b	Off-diagonal entry of the particle covariance matrix. Characterizes the tilt of the ellipse fitting the oil slick.
	c	Second diagonal entry of the particle covariance matrix. Characterizes the stretch of the ellipse fitting the oil slick along the latitudinal direction.
Nominal Second-Order Moments	$\hat{a}$	First diagonal entry of the particle covariance matrix. Characterizes the stretch of the ellipse fitting the oil slick along the longitudinal direction.
	$\hat{b}$	Off-diagonal entry of the particle covariance matrix. Characterizes the tilt of the ellipse fitting the oil slick relative to the nominal oil slick.
	$\hat{c}$	Second diagonal entry of the particle covariance matrix. Characterizes the stretch of the ellipse fitting the oil slick along the latitudinal direction.

influence on the QoIs consisted of oil properties (API, viscosity, IFT) and model parameterizations (wind coefficient, ETG, and water uptake parameter). These six parameters were consequently retained in the GSA.

Table 3 reports the retained uncertainty parameters and the variability ranges extracted from the literature. The choice of prior distributions has a significant impact on the results of PC models, and it is generally considered advantageous to rely on distributions that reflect the prior state of knowledge (Thacker et al., 2015; Wang et al., 2016). Because information on the joint or marginal distributions of the parameters in Table 3 was not available, however, the analysis treated the individual parameters as

uncorrelated and imposed an uninformative prior for each of the parameters considered. Because the parameters had bounded ranges, a uniform prior was consequently selected.

### 3 Polynomial chaos methodology

This section discusses the PC methodology (Wiener, 1938; Ghanem and Spanos, 1991; Le Maître and Knio, 2010) to construct functional representations of QoIs in terms of uncertain inputs. A nonintrusive regularized regression technique outlined in Section 3.1 is applied for this purpose. A brief discussion is provided

TABLE 2 Screening study to shortlist uncertainty parameters of the oil spill model, keeping those of interest to construct surrogate models.

Uncertainty Parameter	Qualitative effects on the weathering and geometry of the oil
API	Affects weathering, limited effect on transport
Pour Point	No observed effect
Asphaltene Content	Little changes in weathering
Dynamic Viscosity	Limited effects on geometry, noticeable changes in dispersion
Interfacial Tension	Noticeable weathering effects causing changes in particle distribution
Spread Coefficient (Fay's Model)	Noticeable effect on oil slick geometry
Spread Coefficient (Empirical Thickness Gradient)	Noticeable effect on oil slick geometry
Emulsification Coefficient	Little effects on weathering and geometry
Water Uptake Parameter	Noticeable effects on weathering
Wind Coefficient	Noticeable effects on oil evaporation, geometry, and transport

Ten input parameters are examined and varied individually, observing the effect of changing one parameter on the quantities of interest. Parameters with a negligible effect were ignored.

**TABLE 3** Uncertainty parameters with variable notation, value range considered in the referenced literature, range selected for constructing the surrogate model, and a brief description of the uncertain input.

Parameter	Variable	Literature Range	Selected Range	Description
API	$\xi_1$	Heavy oil with < 20 (Al-Maamari et al., 2006; Schenk et al., 2006) Light oil with > 40 (Geary, 2017) Medium oil with $\in [20, 40]$ (Lord et al., 2018)	[20, 40]°	The American Petroleum Institute (API) gravity is a commonly used index of the density of crude oil or refined products. The API is inversely proportional to the specific gravity of the hydrocarbon. Oils can be typically classified into light, medium, and heavy oils depending on their (Hollebone, 2014)
IFT	$\xi_2$	[1, 35] dynes (Abdul-Majeed and Abu Al-Soof, 2000) [0.5, 35] dynes approximately (Whitson and R Brule, 2000)	[1, 34]dynes	Two immiscible fluids in contact experience forces at the interface (Ling and He, 2012). These forces are called interfacial tension when both fluids are liquids (Fogang et al., 2020). The potency of this force is characterized by a constant, denoted by IFT, which is a property of the fluids at contact (Deguillard et al., 2013).
ETG	$\xi_3$	[2, 30] (Reed et al., 1995; Reed et al., 1999) [5, 30] (Neves, 1985; Janeiro et al., 2012)	[5, 30]	The Fay oil spread and ETG spread models are both commonly used to estimate the spread of surface oil. Fay (Fay, 1969) proposed a model based on oil spread in a quiescent water body. The ETG model assumes a continuously decreasing oil slick thickness in the radial direction, associating a speed for the spread at the edge of the oil slick
Wind Coefficient	$\xi_4$	[0, 3] % (De Dominicis et al., 2013b,a) [1, 4] % with fine-tuning when needed (Fernandez, 2010) < 6% (Reed et al., 1994; Kako et al., 2011; Maximenko et al., 2012)	[0, 0.06]	Wind at the surface of the sea create shear forces that distort the oil slick at the surface. The wind effect at the surface can be incorporated by adding a fraction of the wind speed to the surface currents. This fraction is called the wind coefficient, which must be calibrated to the motion of passive drifters, such as buoys, to achieve physically consistent results.
Water Uptake Parameter	$\xi_5$	$\approx 2 \times 10^{-5}$ (Mackay and Zagorski, 1981) $\approx 2 \times 10^{-5}$ (Fingas, 1995) $\approx 10^{-6}$ (Wang et al., 2008) $\approx 2 \times 10^{-6}$ (Mishra and Kumar, 2015)	$[1 \times 10^{-6}, 2 \times 10^{-5}]$	Water-in-oil emulsions form when sufficient water is taken up by oil and sufficient energy is provided to promote the emulsion (Fingas and Fieldhouse, 2014). Some of the most widely used models were proposed by Mackay and Zagorski (1981; 1982). The models suggest that emulsification is proportional to the water uptake coefficient, the time the oil spends in water, the fraction of the water content in the oil slick, and the square of the wind speed.
Viscosity	$\xi_6$	[10 – 500]cP (Sanchez-Minero et al., 2014) [0.02 – 1000]cP (Abdul-Majeed et al., 1990) > 0.08cP (Khan et al., 1987)	[0.2, 150]cP	Oil viscosity characterizes the ability of the fluid to resist flowing. The viscosity was correlated with the (Al-Maamari et al., 2006; Alomair et al., 2015)

in Section 3.2 concerning how surrogates are exploited to estimate the global variance-based sensitivities of QoIs to uncertain inputs.

### 3.1 Polynomial chaos expansions

In the PC approach (Knio and Le Maître, 2006; Le Maître and Knio, 2010; Sraj et al., 2017), uncertain inputs are parametrized in terms of a vector of independent canonical random variables,  $\xi$ . The dependence of a generic QoI,  $X$ , on the uncertain inputs is approximated by a truncated series of the following form:

$$X(\xi) \approx \sum_{k=0}^P c_k \Psi_k(\xi), \tag{7}$$

where  $\Psi_k$  denotes the orthogonal basis function defined over the probability space associated with  $\xi$ ,  $c_k$  represents the expansion coefficients to be determined, and  $P + 1$  indicates the size of the approximation basis.

In light of the discussion in Section 2,  $d$  uncertain input parameters are parametrized using  $d$  independent canonical random variables uniformly distributed over  $[-1, 1]^d$ . Thus, the

random vector  $\xi = \{\xi_1, \dots, \xi_d\}$  has components whose physical ranges coincide with those of the associated model parameters in Table 3. The basis functions ( $\Psi$ ) are the multidimensional Legendre polynomials in the random vector  $\xi$ . A generic input parameter is expressed as  $p_i(\xi) = \mu_i + \sigma_i \xi_i$  for  $i = 1, \dots, d$ . In this formulation,  $\mu_i = \frac{1}{2}(a_i + b_i)$  denotes the nominal value of  $p_i$ ,  $\sigma_i = \frac{1}{2}(b_i - a_i)$  represents half its range, and  $a_i$  and  $b_i$  represent the lower and upper bounds of the physical range of  $p_i$ , respectively. We adopted a total order truncation technique so that the truncated basis size is as follows:

$$P + 1 = \frac{(d + p)!}{d! p!},$$

where  $p$  denotes the maximal polynomial degree of the truncated expansion.

PC expansions are generally classified as global or local depending on the span of the stochastic space covered by the model (Najm, 2009). In the present study we focus on global PC models, rely on a so-called non-intrusive methodology to determine the PC coefficients (Eldred, 2009; Lüthen et al., 2021). This indicates that the coefficients are determined using the outputs deterministic

forward model runs, performed at suitable realizations of the uncertain inputs. An overview of different methods to generate PC surrogate models could be found in (Najm, 2009; Hadigol and Doostan, 2018; Lüthen et al., 2021).

In preliminary work, we investigated constructing surrogates using projection-based methods based on Gauss and Gauss–Kronrod–Paterson quadratures (Laurie, 1997) and regularized regression following the least absolute shrinkage and selection operator (LASSO) algorithm (Tibshirani, 1996; Roth, 2004; Ranstam and Cook, 2018). The study suggested that surrogates obtained using the LASSO regression yielded lower reconstruction errors than the pseudospectral projection counterparts. The large errors in the projection-based surrogates were due to the noisy particle approximations of the QoIs. Because the regression approach is robust to noisy estimates, it was adopted to construct the surrogates and support the GSA. Note that several open source libraries such as UQ toolkit (Debusschere et al., 2017) and UQLab (Marelli and Sudret, 2014) provide implementations of projection and regression methods that can be readily used to efficiently build PC surrogates.

In the LASSO regression, the coefficients are obtained by minimizing the sum of residuals between the observed variable and PC expansion prediction, and an  $\ell_1$  regularization term is introduced to prevent overfitting. The functional to be minimized is as follows:

$$R(c_k) = \left( \frac{1}{2N} \sum_{i=1}^N \left( y_i - \sum_{k=0}^P c_k \Psi_k(\xi^{(i)}) \right)^2 + \lambda \sum_{k=1}^P |c_k| \right), \quad (8)$$

where  $N$  represents the number of observations,  $y_i$  indicates the QoI at observation  $i$ ,  $\xi^{(i)}$  denotes the  $i^{th}$  observation point, and  $\lambda$  represents a positive regularization constant to be determined. The LASSO algorithm is applied with 10-fold cross-validation to estimate the model error (Obuchi and Kabashima, 2016). The optimal value of  $\lambda$  yields the smallest cross-validation mean squared error. Once determined, the corresponding coefficient vector is adopted to define the PC surrogate.

### 3.2 Global sensitivity analysis

The Sobol indices estimate the influence of the input uncertainties on the variability in the model output by evaluating the ratio of the conditional variances to the total variance of the output. Using the same notation as in the work by (Crestaux et al., 2009), the sensitivity index corresponding to the index set  $i \subset D \equiv \{1, \dots, d\}$  are defined as:

$$S_i \equiv \frac{V_i(X)}{V(X)} = \frac{E[X^2(\xi_i)]}{V(X)} \quad (9)$$

whereas the corresponding total sensitivity index is defined according to:

$$T_i \equiv \frac{E_{\xi_{-i}}[V_{\xi_i}(X|\xi_{-i})]}{V(X)}, \quad (10)$$

where  $X$  is a generic QoI,  $d$  is the total number of dimensions,  $E$  and  $V$  denote the expectation and variance operators, respectively, and  $\sim i$  represents the complement of the subset  $i$  in  $D$ .

The Sobol sensitivity indices could be estimated efficiently using the PC expansion by exploiting the orthogonality of the PC basis (Sobol, 1993; Homma and Saltelli, 1996; Sobol, 2001; Sudret, 2008; Crestaux et al., 2009; Le Maître and Knio, 2010; Alexanderian et al., 2012). The Sobol indices are given by:

$$S_i \approx \frac{\sum_{k \in S_i} c_k^2 \|\Psi_k\|_2^2}{\sum_{k \geq 1} c_k^2 \|\Psi_k\|_2^2}, \quad (11)$$

where  $S_i = \{k \mid \Psi_k \text{ has degree } 0 \text{ in all } \xi_j \text{ with } j \notin i\}$ . Similarly, the total sensitivity index corresponding to the singleton  $\{i\}$  can be readily obtained using:

$$T_i \approx \frac{\sum_{k \in T_i} c_k^2 \|\Psi_k\|_2^2}{\sum_{k \geq 1} c_k^2 \|\Psi_k\|_2^2}, \quad (12)$$

where  $T_i = \{k \mid \Psi_k \text{ has degree } > 0 \text{ in } \xi_i\}$ . Note that the Sobol indices  $S_i$  account for the so-called direct contributions of the uncertain parameters  $\xi_i$ , and that  $T_i$  accounts for both the direct contributions of the uncertain variable  $\xi_i$  as well as its mixed interactions with the remaining variables. In particular, it can readily be seen that a small  $T_i$  justifies neglecting  $\xi_i$  and according restricting the uncertain input space.

## 4 Results and discussion

### 4.1 Assessment of the surrogate model

The  $N = 600$  realizations ( $\xi^{(i)}$ ) of the random germ ( $\xi$ ) were generated using a Latin hypercube sampling algorithm to generate PC surrogates. The same realizations of the germ were used for each of the eight considered scenarios, and MOHID was applied to simulate the evolution of the corresponding spills. As discussed in the previous section, PC surrogates of the selected QoIs were determined by solving the LASSO regression problem based on the simulation outputs. This section analyzes the performance of the PC surrogates by computing the associated time-dependent normalized  $\ell_2$  errors:

$$E_2(t) = \frac{\sqrt{\frac{1}{N} \sum_{i=1}^N (f(\xi^{(i)}, t) - \hat{f}(\xi^{(i)}, t))^2}}{\left( \max_{\xi} f(\xi, t) - \min_{\xi} f(\xi, t) \right)}, \quad (13)$$

where  $f$  denotes a generic QoI obtained from the MOHID simulation,  $\hat{f}$  is the corresponding QoI approximated by the PC surrogate, and the maximum and minimum function values are defined over all realizations and simulation times in the order indicated. PC surrogate models ranging from first to sixth total order expansions were constructed, and their reconstruction errors were evaluated. The fifth-order PC model was selected because it offered the best compromise between suitable reconstruction errors and computational time. Consequently, the study presents results obtained using a degree five total order truncation.

An illustration of the performance of the PC surrogate is provided in Figure 2A, which depicts the evolution of C Lon and C Lat for a randomly selected realization of  $\xi$ . The results for release Location 1 are used, and curves are generated for winter and summer release scenarios using the MOHID outputs and corresponding PC surrogates. The PC representation errors are depicted in Figure 2B. As expected, errors corresponding to C Lon and C Lat increase with time for both release seasons. Nonetheless, the  $E_2$  metric remains below 6% throughout the simulation period, indicating that the PC representation remains suitable for estimating sensitivities over the entire simulation time, which is reflected in the close alignment between the curves in Figure 2A.

We also analyzed the maximum values over time of  $E_2$  for all considered QoIs and all release scenarios; see Supplementary Table S1. Overall, the results exhibit small error values and alignment between the surrogate and the MOHID predictions for the various realizations, indicating that the PC surrogate suitably represents the functional dependence of the QoIs on uncertain inputs.

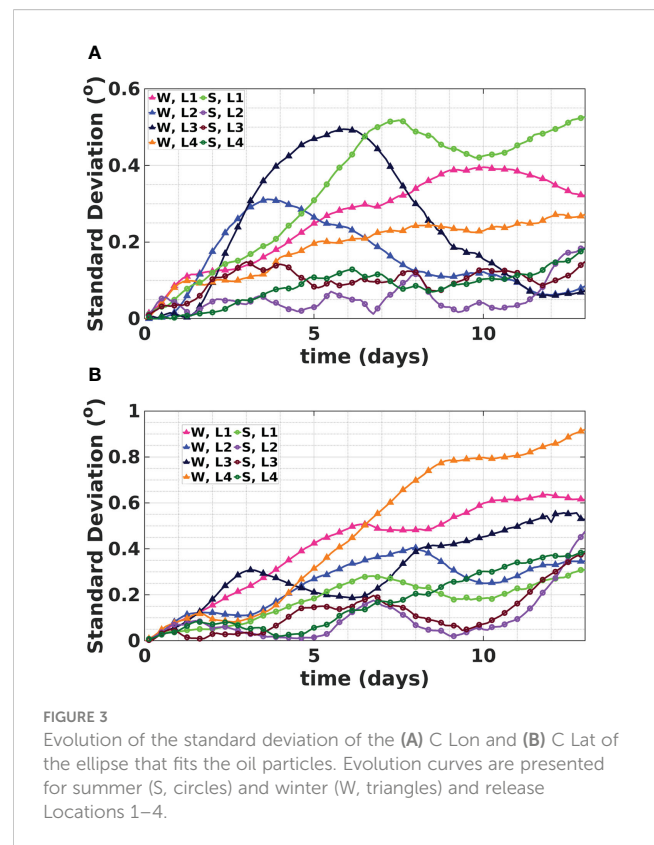
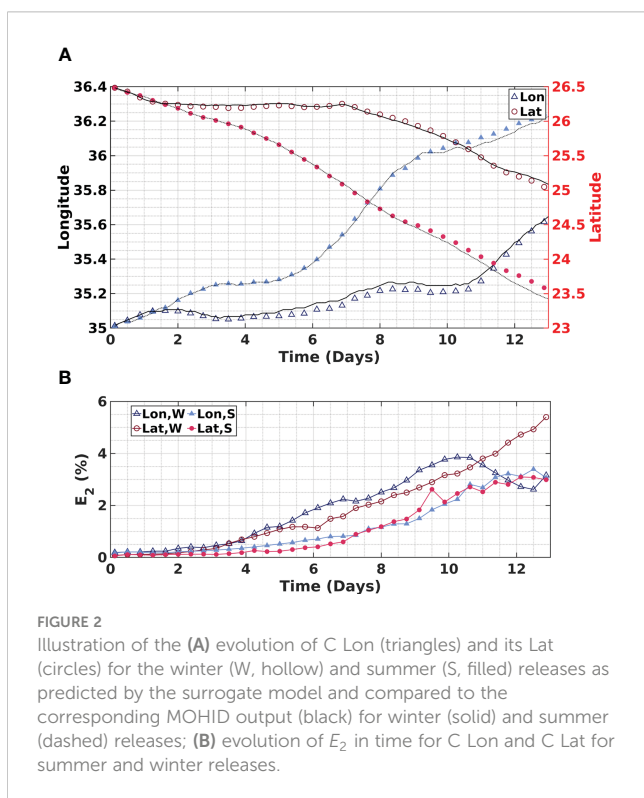
### 4.2 Spill motion and deformation

Figures 3A, B illustrate the evolution of the standard deviation of C Lon and C Lat, respectively. Curves are generated for all eight considered scenarios. The results indicate that C Lon and C Lat generally experience substantial variability, with values of the standard deviation exceeding 0.250 in all scenarios. In addition, C Lat generally exhibits greater variability during the winter scenarios,

attributed to the more chaotic nature of the RS flow field during the selected winter events. A more chaotic flow leads to higher variability (Zhan et al., 2016).

The figures also demonstrate that the standard deviation of C Lat is greater than that of C Lon, which may be attributed to the topography of the RS basin with a greater extent along the latitude. The evolution of the standard deviation is generally nonmonotonic because of the stretching and folding of the oil slick by the ocean eddies. This nonmonotonic behavior has important implications for analyzing sensitivities, as discussed below. Finally, the figures indicate strong variability across release scenarios for C Lon and C Lat, which indicates that different metocean conditions along the RS basin strongly affect the motion of the spilled oil and significantly affect the evolution of parametric uncertainties. These findings may be readily appreciated by contrasting the mean displacements and their variabilities across the eight considered scenarios. The present observations also underscore the importance of using accurate wind information in oil spill modeling (Keramea et al., 2021).

Figure 4 depicts the particle distributions corresponding to four randomly selected realizations of the parameters. The distributions are plotted two weeks after the initial release. Simulations corresponding to a summer release scenario originating at Location 2 are used for this purpose. The distributions reveal that for two out of the four selected realizations of  $\xi$ , C Lat is around 18.25°N (frames b and c), whereas for the other two realizations of C Lat is around 17.5°N (frames a and d). The illustrations correspond to samples at



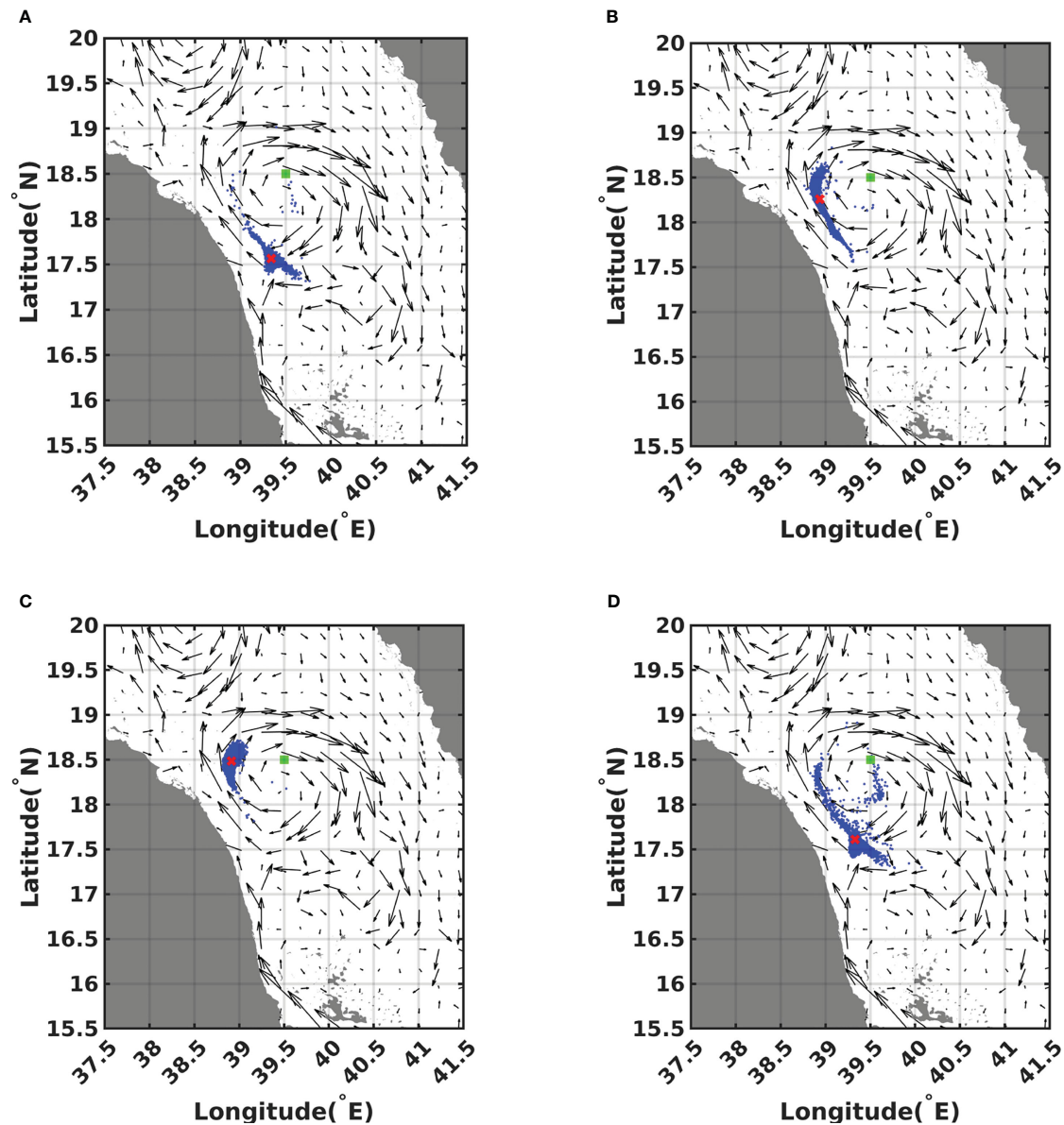


FIGURE 4

Particle distributions at the last simulation time step (14 days from release) for four realizations of the random germ  $S_{xiS}$ . The distributions are plotted individually and presented in frames (A–D). All simulations correspond to a release occurring during summer from release Location 2. Each frame presents the release source location (green square), oil particles (blue dots), and their center of gravity (red cross). Particles are distributed differently for various combinations of uncertainty parameters. Specifically, for some realizations, the center of gravity is located at a similar latitude as the initial release (frames B, C), whereas for others, the center of gravity is located noticeably southward of the initial release (frames A, D).

the modes of C Lat for the summer release scenario with an initial release from Location 2. The particle distributions also illustrate the variability resulting from using *different inputs* with the *same metocean conditions*, see also Figure S2, which depicts the evolution of the PDFs of C Lon and C Lat revealing multimodal behavior. This highlights the importance of properly selecting key model parameters and physical oil properties and accounting for residual uncertainties.

Figures 5A, B display the evolution of the total sensitivity indices for C Lon and C Lat for all release locations. The curves are depicted for the summer release scenarios. The results for the winter scenarios were similar and, thus, omitted. The results indicate that the wind coefficient has the greatest influence on the location of the oil spill

centroid. Around Day 9, the sensitivity of C Lon and C Lat with respect to the viscosity briefly rises, but this behavior is insignificant because the variances drop to small values around that time. Similar behavior also occurs with IFT and approximately 10 days after the initial release of oil. These results imply that, among the investigated parameters, the wind coefficient is the dominant input parameter affecting the transport of an oil spill.

These findings are consistent with and enhance well-established results in the literature, which have demonstrated that the transport of surface oil is strongly influenced by wind speed and direction and that wind stresses tend to elongate the surface of the oil slick in the direction of the surface winds (Androulidakis et al., 2018; Lodise et al., 2019;

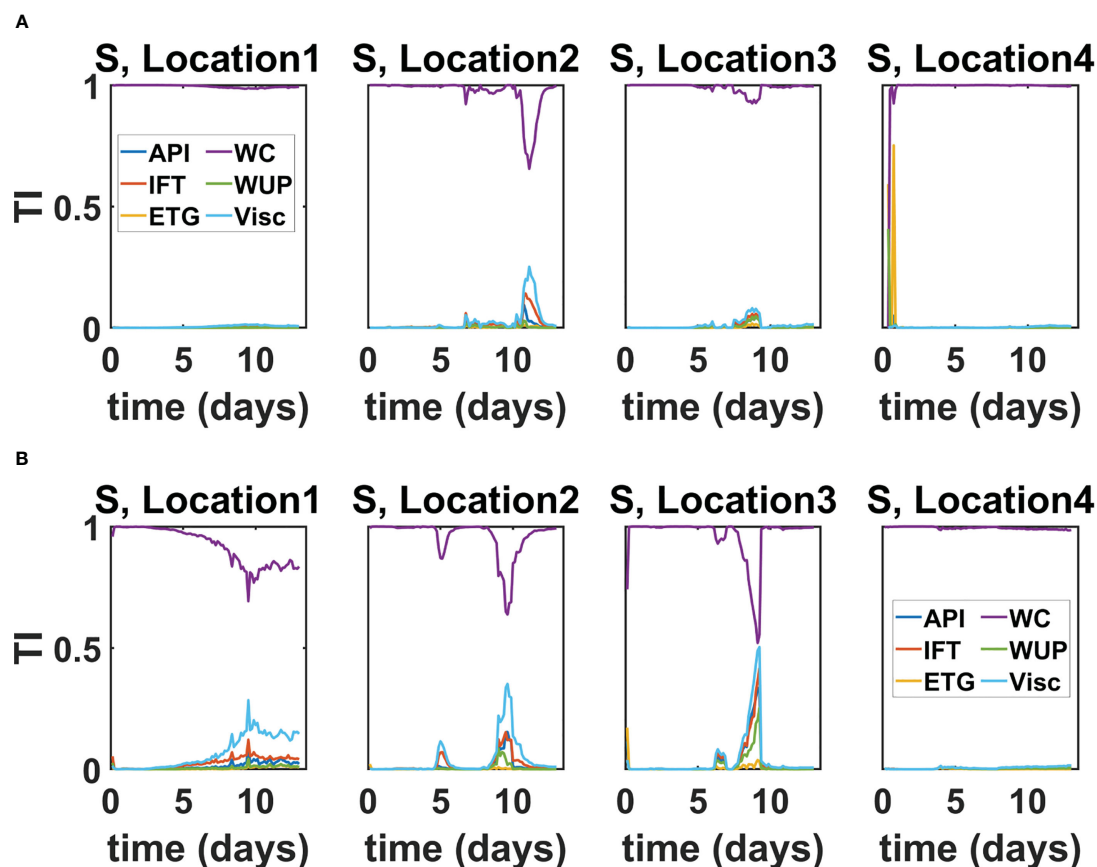


FIGURE 5 Evolution of the TI of (A) C Lon and (B) C Lat. Evolution curves are presented for the summer release scenarios from Locations 1–4.

Duran et al., 2021). Our results provide quantitative estimates of the contribution of the uncertain variables on the location of the center of volume of the oil slick and allows to rule out uncertain parameters with lower contribution to the variability in the location of the center of volume. These results not only reveal that uncertainties in the wind coefficient dominate uncertainties in transport, but also indicate that all other uncertain parameters have a negligible contribution to the observed variabilities. Therefore, for the sake of predicting oil transport and estimating relevant confidence bounds, one could restrict the input space to the wind coefficient only, thus disregarding the remaining uncertain parameters.

The geometry of the oil slick is characterized using the central particle moments  $a$ ,  $b$ , and  $c$ . We analyzed the variances of  $a$ ,  $b$ , and  $c$  and generally observed that the prevailing behavior for C Lon and C Lat also holds for the second-order central particle moments. Figures 6A–C illustrate the evolution of the standard deviation of  $a$ ,  $b$ , and  $c$  over the two-week release period. The curves outline a general increase in the variability of the central particle moments over time, except for the summer release scenario originating from release Location 3, which exhibits large oscillations. These oscillations may arise because the original release location is at the periphery of an eddy, inducing a rotational motion about its core.

The standard deviation of  $a$  is significantly smaller than that of  $c$ , which may be attributed to the elongated shape of the RS basin. For a given spill scenario (i.e., when the spill location and metocean

conditions are specified), the variability of all three second moments is dominated by the uncertainty of the wind coefficient. This result can be readily appreciated from Figure 7, displaying the evolution of the total sensitivity indices of the central particle moments for the summer release scenarios. Locations 1 and 2 display a nonmonotonic change in the total sensitivity, with the wind coefficient having the largest influence. This outcome is unsurprising because the shear stresses imposed by the surface winds stretch the oil slick along the main wind direction, directly distorting its shape (Kampouris et al., 2021). However, the effects of the IFT and viscosity are generally not negligible, as observed from the results for Locations 1 and 2. Empirical findings have suggested that more-viscous oils spread less than less-viscous oils (Olugbenga et al., 2020), explaining the observed sensitivity of the slick deformation to the oil viscosity. Moreover, the IFT directly influences surface oil spreading, ultimately affecting the shape of the oil slick and how it stretches under the action of surface currents (Winoto et al., 2014; Speight, 2020). These results indicate that uncertainties about the shape of the oil slicks are primarily dependent on the wind coefficient and to a lesser degree on IFT and viscosity, and that the contribution of the remaining parameters is negligible.

As discussed in Section 2.3, we rely on the second-order nominal particle moments,  $\hat{a}$ ,  $\hat{b}$ , and  $\hat{c}$  to characterize the properties of the elliptical region, centered at the centroid of the nominal oil slick, where spilled oil is likely to be present. Figures 6D–F illustrate the evolution of the standard deviation of  $\hat{a}$ ,  $\hat{b}$ , and  $\hat{c}$  for all release

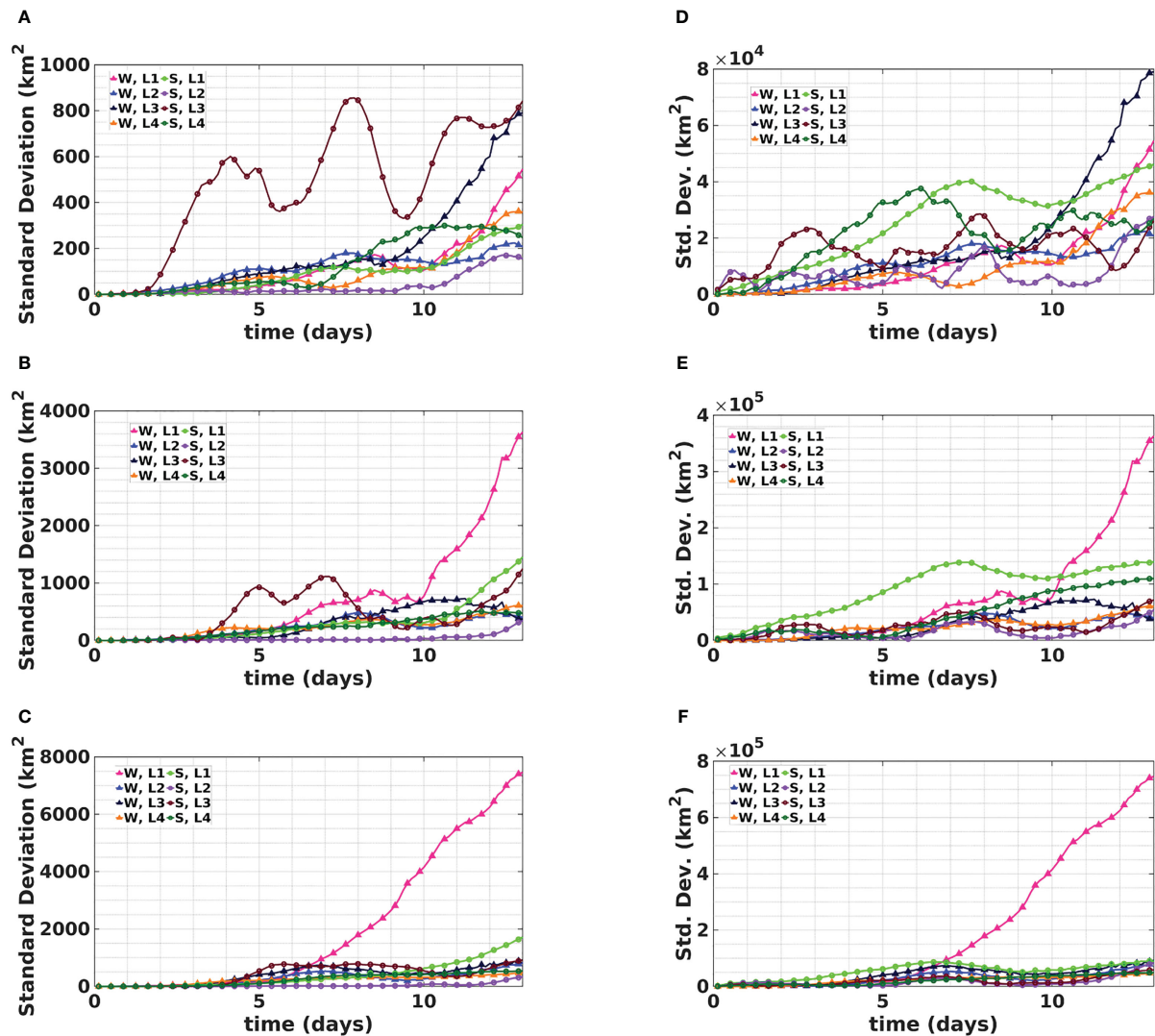


FIGURE 6 (A–C) Evolution curves of the standard deviation of the “a”, “b”, and “c” variables for all considered release scenarios. (D–F) Evolution of the standard deviation of  $\hat{a}$ ,  $\hat{b}$ , and  $\hat{c}$  for the summer release scenarios.

scenarios. The evolution of the standard deviation of the nominal moments is similar to that of the central moments; however, the magnitude of the nominal particle moments is much larger than that of the central particle moments. This result is expected because the central particle moments measure the extent of the oil slick, whereas the nominal particle moments characterize the extent of the region centered on the centroid of the nominal oil slick, where individual oil slick realizations are likely to be present. The latter may be well separated from the nominal oil slick, explaining the higher values of the second-order nominal particle moments.

Unlike the variability of the central moments, which primarily depends on the wind coefficient and to lesser extent IFT and viscosity, the variability of the nominal moments is controlled by the wind coefficient. The total sensitivity indices (not shown) corresponding to the wind coefficient are approximately 1 for the entire simulation duration, and the remaining uncertainty parameters have total sensitivities close to zero. This behavior is unsurprising because the nominal moments reflect the combined

effects of deformation (substantially affected by the wind coefficient) and mean motion (controlled by the wind coefficient). This approach substantially filters out the effects of IFT and viscosity, whose influence on the variability of the nominal moments can be deemed negligible. Thus, uncertainties in the second-order nominal particle moments are dominated solely by the wind coefficient.

### 4.3 Weathering quantities

This section analyzes the variability of the FME and FMD. The evolution of the standard deviation of the FME is reported in Figure 8A for all release scenarios. The figure indicates that the standard deviation of the FME increases monotonically as time progresses over a two-week period, with considerable variance after one week of the initial release. On the other hand, these predictions are fairly similar for the various release scenarios. As can be seen in Figure S3, the PDFs of FME also exhibit similar profiles, with widths increasing over time.

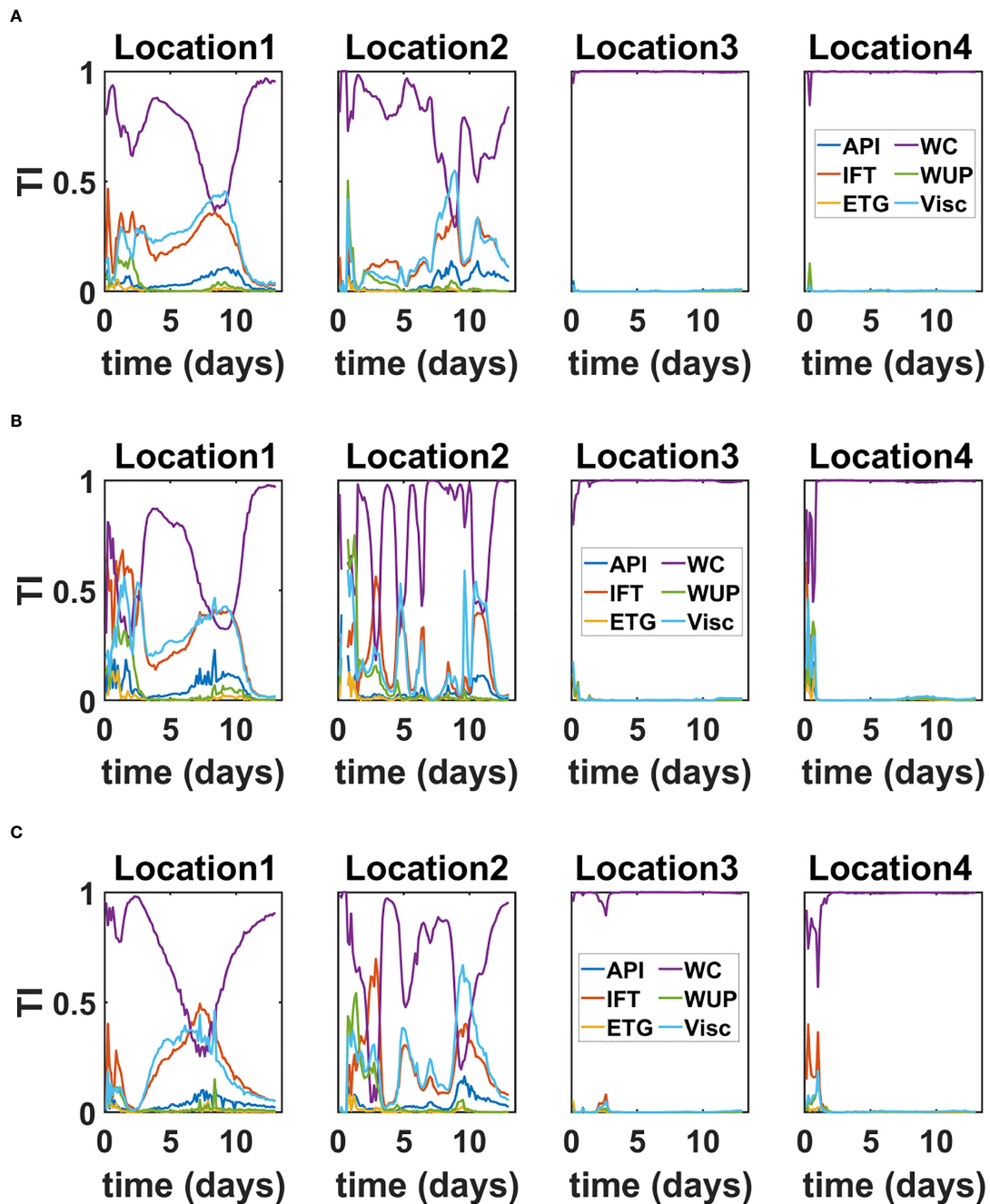
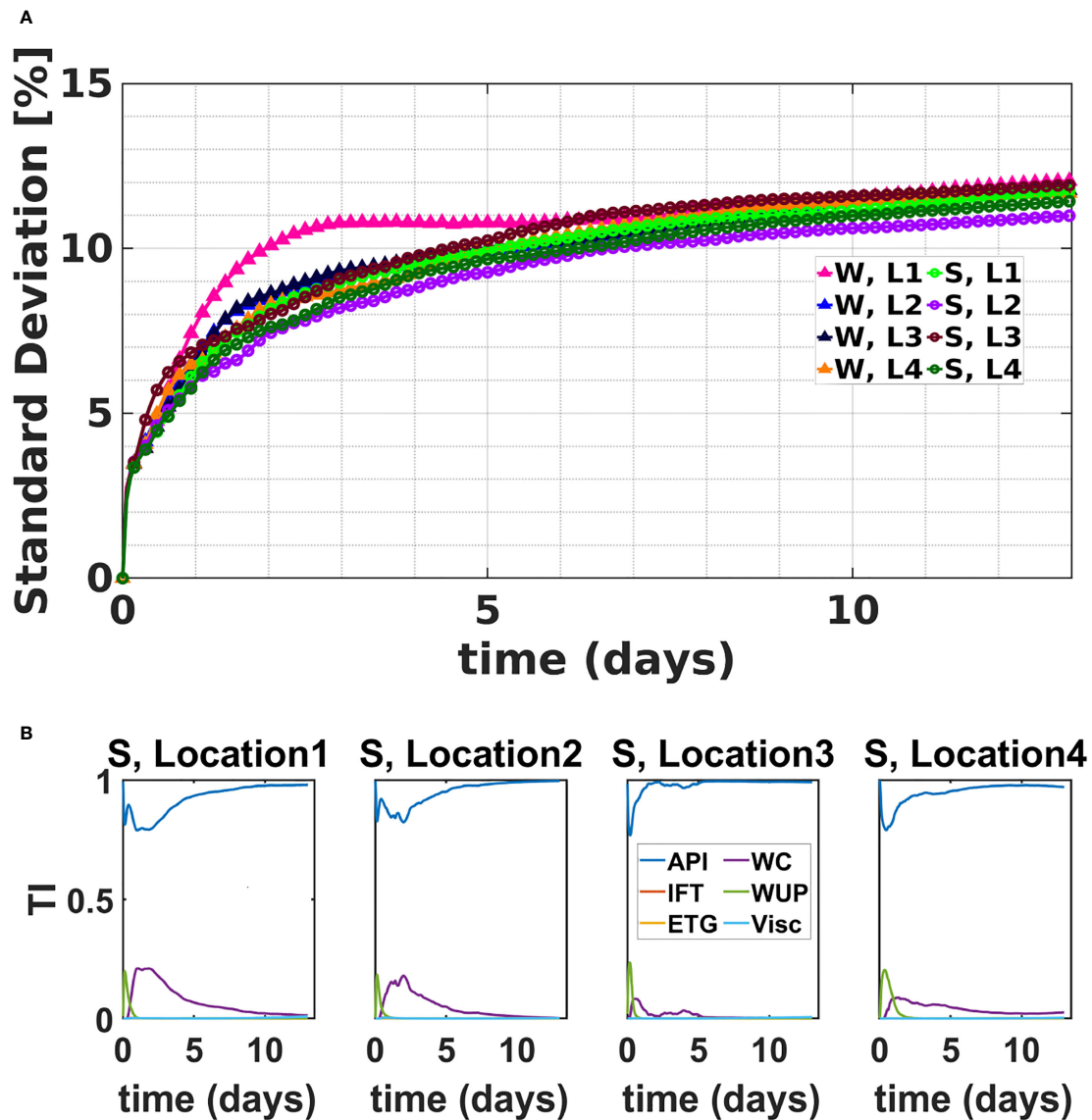


FIGURE 7 (A–C) Evolution curves of the total sensitivity indices corresponding to variables “a”, “b” and “c”, respectively, for the summer release scenarios.

The evolution of the total sensitivity indices for the summer release scenarios is presented in Figure 8B. The curves demonstrate that, except for a short time following the release, the FME is most sensitive to the oil's API. The total sensitivity indices corresponding to the wind coefficient also appear to be more significant than the other uncertainty parameters; however, the influence of the wind coefficient on the FME is secondary compared to the API. These observations are consistent with the findings by (French-McCay et al., 2021), and also indicate that except at early times following the release, the variance of FME is dominated by uncertainty in API, and that contributions from other sources can be neglected.

Figure 9 presents a scatterplot of the 600 FME values predicted by MOHID one week after the initial release of oil from Location 1 for the winter and summer scenarios. The figure also illustrates the conditional expectation of FME and the 10<sup>th</sup> and 90<sup>th</sup> percentiles for varying obtained from the PC surrogate. The plots reveal that the FME increases nearly linearly with increasing. Realizations falling below the 10<sup>th</sup> percentile curves exhibit a larger scatter compared with realizations falling above the 90<sup>th</sup> percentile curves. This result is consistent with the skewness of the PDFs and the structure of their tails (see Figure S3). We examined the origin of these events by examining their parameters. The analysis indicated that extreme



**FIGURE 8** Evolution of the (A) standard deviation of the FME in time for all release scenarios considered. Subplot (B) illustrates the evolution of the total sensitivity indices of the FME corresponding to the summer release scenarios.

FME values correlate with extreme values of the wind coefficient. As expected, due to convective effects induced by surface winds, low FME values occur for low values of the wind coefficient and vice versa for higher wind coefficient values, which aligns with the results from (Saltymakova et al., 2020).

Figure 10A illustrates the evolution of the standard deviation of the FMD for all considered release scenarios. The figure indicates that the standard deviation of the FMD increases monotonically over time. The standard deviation estimated from the PC surrogate is comparable to the empirical standard deviation; however, the empirical standard deviation is smoother than that of the PC surrogate, possibly due to the cross-validation strategy adopted to obtain the PC coefficients. The results also reveal that the standard deviations vary substantially across various release scenarios, indicating that uncertainty in the input parameters over the considered ranges leads to appreciable relative differences in the FMD estimates. Overall, however, the FMD estimates

exhibit small values in all scenarios considered, despite the large coefficients of variation. This is consistent with the empirical PDFs plotted in Figure S4. In contrast to the FME, the FMD PDFs reveal long-tailed unimodal distributions peaking at a small values (< 1%).

The evolution of the total sensitivity indices of the FMD for all summer release scenarios is presented in Figure 10B. Initially, the IFT exhibits the highest total sensitivity index. As time progresses, the total sensitivity index of the IFT decreases to just below 0.5; thus, the IFT remains significant throughout the release. The FMD is also initially sensitive to the water uptake parameter after the oil release; however, it becomes insignificant later. The sensitivity of the FMD to viscosity increases with time, and the total sensitivity index of viscosity becomes the largest parameter and remains so over the remaining simulation time. Because the standard deviation of the FMD is very small in the first two days following the release, for the range of considered scenarios, the variability of the FMD is primarily sensitive to

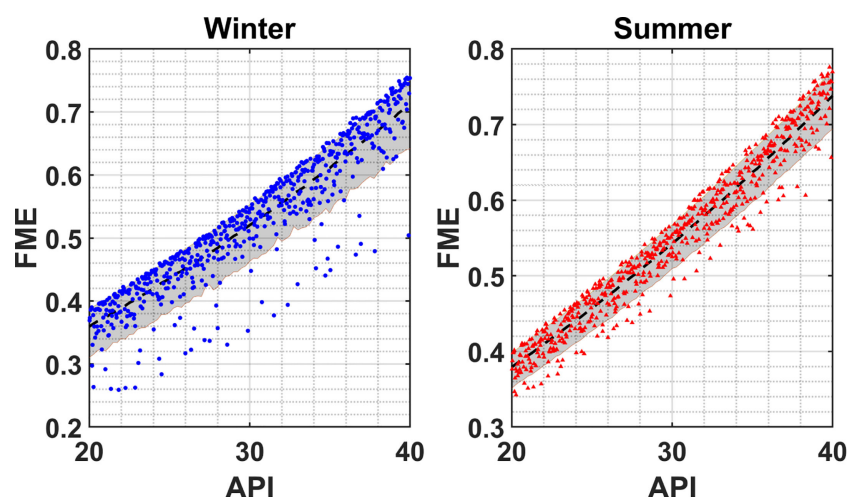


FIGURE 9

Scatterplot of the FME value one week after the initial release of oil from Location 1 for the summer and winter release scenarios, as predicted by MOHID. The figure also portrays the projection of the mean (black dashed line) and the 10<sup>th</sup> (lower boundary of the shaded area) and 90<sup>th</sup> (upper boundary of the shaded area) percentiles of the FME for values.

viscosity and IFT. The sensitivity of the FMD to the IFT may also be anticipated because the IFT affects the oil breakup dynamics and, consequently, the dispersion into the water column, as suggested from the observations by (Delvigne and Sweeney, 1988).

Note in the cases of FME and transport QoIs the analysis revealed the presence of a dominant parameter, but in the case of FMD multiple parameters have significant contributions to the variance. This leads us to examine the behavior of higher order sensitivities in this instance. Figure S5 illustrates the evolution of the first-order and second-order Sobol sensitivity indices for FMD. The results indicate that in addition to direct contributions from the uncertainty in IFT and viscosity, the mixed (cross-sensitivity) term between the IFT and viscosity also has significant impact. Thus, the contributions of these two dominant sources of uncertainty are clearly not additive.

A summary of the GSA results for the summer scenarios is presented in Table 4. The table presents the average total sensitivity index for each QoI for each uncertainty parameter for the summer releases, respectively. As indicated, the total sensitivities are averaged over the release locations and across various time spans. Specifically, sensitivity values are averaged over early ( $\leq 3$  days), intermediate ( $> 3$  and  $< 10$  days), and late ( $\geq 10$  days) integration periods to further aid in identifying the uncertain input to which the QoI is most sensitive. Consistent with earlier discussions, for all considered time ranges, the location and geometry of the oil slick are most sensitive to the wind coefficient, and the variability of the FME is predominantly affected by the API. In contrast, the FMD exhibits strong sensitivity to viscosity and IFT. The results corresponding to the winter release exhibited similar behaviors and are presented in Table S2.

## 5 Conclusion

We considered eight scenarios for oil spill incidents in the RS by specifying four release locations and two metocean conditions characteristic of winter and summer. For each scenario, the

evolution of the released oil is simulated using the MOHID oil spill model over two weeks following the release.

Six uncertainty parameters that strongly influence the evolution of the oil were selected following a preliminary screening study. The six uncertain inputs include oil properties and oil-model parameters, including the API gravity (API), interfacial tension (IFT), empirical thickness gradient (ETG), wind coefficient (WC), water uptake parameter (WUP), and viscosity. We constructed PC surrogates of QoIs characterizing the location and geometry of the slick as well as weathering effects. A nonintrusive, regularized regression approach was used for this purpose. We analyzed the suitability of the surrogate models by quantifying the representation errors and exploited them to investigate the variability, distribution, and sensitivity of the QoIs.

In particular, the study indicated that, for the range of considered scenarios, QoIs characterizing the motion and deformation of the oil slick generally have large variances and exhibit strong dependence on metocean conditions. For a given scenario, the analysis demonstrated that the wind coefficient generally controls the influence of the motion and deformation of the oil slick. Specifically, the wind coefficient governs the variability in the centroid and nominal particle moments of the oil slick. The effects of viscosity and IFT are not negligible to determine the variability of the central particle moments. The analysis also indicated that the variability of FME is controlled by the API, with higher FME values for summer scenarios than for winter scenarios, as expected. Extreme values of the FME are positively correlated with extreme values of the wind coefficient. Finally, the results indicate that the variability of the FMD primarily depends on the oil viscosity followed by the IFT.

Overall, the present experiments indicate that, for the considered conditions, the prediction of areas affected by an accidental oil spill depends on metocean conditions and is highly sensitive to uncertainties in the metocean field and wind-coupling parametrization. For the range of tested conditions, the amount of oil affecting a region may be substantially affected by oil evaporation, which is highly sensitive to the API. For the assessment of spill effects over relatively short periods

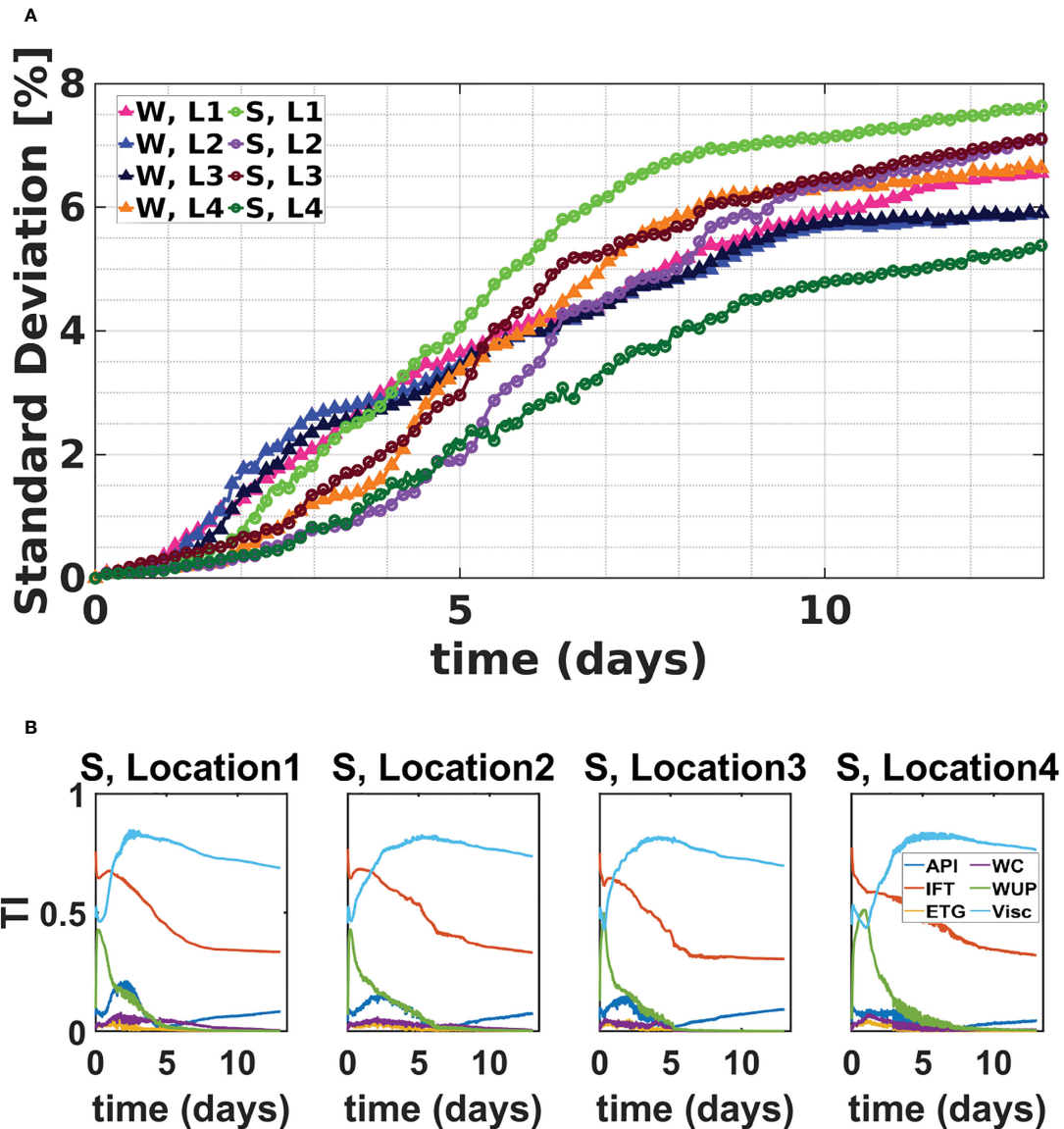


FIGURE 10 Evolution of the (A) standard deviation of the FMD in time. This plot presents the results for all considered release scenarios. Subplot (B) illustrates the evolution of the total sensitivity indices of the FME corresponding to the summer release scenarios.

TABLE 4 Table listing the average total sensitivity indices for short ( $\leq 3$  days), intermediate ( $> 3$  days and  $< 10$  days), and long ( $\geq 10$  days) term.

		API	IFT	ETG	WC	WUP	Visc
FMD	$t \leq 3$	0.11225	0.62574	0.028801	0.04101	0.24731	0.63961
	$3 < t < 10$	0.042218	0.41732	0.006038	0.019015	0.031412	0.78574
	$t \geq 10$	0.064339	0.3296	0.001439	0.006212	0.00344	0.73624
FME	$t \leq 3$	0.87997	0.00078	0.000291	0.090411	0.031802	0.000709
	$3 < t < 10$	0.96435	0.00034	4.06E-05	0.034939	0.001012	0.000597
	$t \geq 10$	0.98456	0.001564	6.93E-05	0.011619	0.001523	0.003301
C Lon	$t \leq 3$	0.000955	0.00726	0.015054	0.98725	0.005222	0.00056
	$3 < t < 10$	0.002996	0.00559	0.000986	0.99151	0.002528	0.008226

(Continued)

TABLE 4 Continued

		API	IFT	ETG	WC	WUP	Visc
	$t \geq 10$	0.005914	0.013128	0.001296	0.96885	0.001726	0.026242
<b>C Lat</b>	$t \leq 3$	0.001705	0.002053	0.002319	0.99533	0.001196	0.001364
	$3 < t < 10$	0.0191	0.026885	0.002147	0.95025	0.010396	0.047219
	$t \geq 10$	0.010077	0.017942	0.003118	0.94284	0.00455	0.0516
<b>a</b>	$t \leq 3$	0.014952	0.089145	0.008293	0.91344	0.046241	0.069087
	$3 < t < 10$	0.022201	0.10196	0.002737	0.85138	0.007729	0.12626
	$t \geq 10$	0.026967	0.072676	0.002187	0.88324	0.003541	0.076154
<b>b</b>	$t \leq 3$	0.03867	0.2049	0.024025	0.79452	0.08919	0.14753
	$3 < t < 10$	0.021553	0.10676	0.004159	0.86079	0.010572	0.1124
	$t \geq 10$	0.021521	0.068708	0.002967	0.89682	0.00577	0.081479
<b>c</b>	$t \leq 3$	0.01493	0.12443	0.011497	0.84562	0.075593	0.079597
	$3 < t < 10$	0.020627	0.11939	0.003532	0.81426	0.008395	0.12839
	$t \geq 10$	0.023634	0.068933	0.001546	0.89621	0.004381	0.078065

The quantity of interest results are indicated along the leftmost column, and the uncertainty parameters are indicated along the top row. The results correspond to the summer scenarios, averaged across all release locations.

following an accidental release, these findings suggest that effective approaches can be conceived that focus primarily on metocean conditions, wind effects, evaporation, and their associated variabilities.

In conclusion, the present analysis focused on the influence of uncertainties in key oil properties and model parametrizations and ignored other sources of uncertainty, such as those affecting metocean conditions. In future work, we plan to account for these uncertainties using a flow ensemble approach while leveraging the results of the present study to restrict the number of uncertain oil and model parameters to a reasonably sized set. This plan would enable efficient means to simultaneously address forecasting and parameter uncertainties and effectively capitalize on the resulting predictions for impact assessments, source identification, or decision support.

## Data availability statement

The raw data supporting the conclusions of this article will be made available by the authors, without undue reservation.

## Author contributions

Conceptualization, MH, HM, and OK; Methodology, MH, HM, and OK; software, MH; validation, OL, IH, and OK; formal analysis, MH, HM, and OK; investigation, MH, HM, and OK; resources, IH and OK; data curation, MH and HM; writing—original draft preparation, MH, HM, and OK; writing—review and editing, MH, HM, OL, IH, and OK; visualization, MH and HM; supervision, OL, IH, and OK; project administration, OL, IH, and OK; funding acquisition, IH and OK. All authors contributed to the article and approved the submitted version.

## Funding

This publication is based on work supported by the King Abdullah University of Science and Technology (KAUST) Office of Sponsored Research (OSR) under Award No. OSR-CRG2018-3711 and the Virtual Red Sea Initiative Award No. REP/1/3268-01-01.

## Conflict of interest

The authors declare that the research was conducted in the absence of any commercial or financial relationships that could be construed as a potential conflict of interest.

## Publisher's note

All claims expressed in this article are solely those of the authors and do not necessarily represent those of their affiliated organizations, or those of the publisher, the editors and the reviewers. Any product that may be evaluated in this article, or claim that may be made by its manufacturer, is not guaranteed or endorsed by the publisher.

## Supplementary material

The Supplementary Material for this article can be found online at: <https://www.frontiersin.org/articles/10.3389/fmars.2023.1185106/full#supplementary-material>

## References

- Abdul-Majeed, G. H., and Abu Al-Soof, N. B. (2000). Estimation of gas-oil surface tension. *J. Petroleum Sci. Eng.* 27, 197–200. doi: 10.1016/S0920-4105(00)00058-9
- Abdul-Majeed, G. H., Kattan, R. R., and Salman, N. H. (1990). New correlation for estimating the viscosity of undersaturated crude oils. *J. Can. Petroleum Technol.* 29, 80–85. doi: 10.2118/90-03-10
- Adetula, B., and Bokov, P. (2011). “Method for calculation of global sensitivity indices for few-group cross-section-dependent problems,” in *International Conference on Mathematics and Computational Methods Applied to Nuclear Science and Engineering (M&C 2011)*, Rio de Janeiro, RJ, Brazil, American Nuclear Society (ANS).
- Alexanderian, A., Winokur, J., Sraj, I., Srinivasan, A., Iskandarani, M., Thacker, W. C., et al. (2012). Global sensitivity analysis in an ocean general circulation model: a sparse spectral projection approach. *Comput. Geosciences* 16, 757–778. doi: 10.1007/s10596-012-9286-2
- Alkhashal, H., and Westcott, B. (2019). *Iranian Oil tanker hit by two missiles near Saudi port: state news* (Jeddah, Saudi Arabia: CNN).
- Al-Maamari, R. S., Houache, O., and Abdul-Wahab, S. A. (2006). New correlating parameter for the viscosity of heavy crude oils. *Energy Fuels* 20, 2586–2592. doi: 10.1021/ef0603030
- Alomair, O., Jumaa, M., Alkorieem, A., and Hamed, M. (2015). Heavy oil viscosity and density prediction at normal and elevated temperatures. *J. Petroleum Explor. Production Technol.* 6, 253–263. doi: 10.1007/s13202-015-0184-8
- Androulidakis, Y., Kourafalou, V., Özgökmen, T., Garcia-Pineda, O., Lund, B., Le Hénaff, M., et al. (2018). Influence of river-induced fronts on hydrocarbon transport: a multiplatform observational study. *J. Geophysical Research: Oceans* 123, 3259–3285. doi: 10.1029/2017JC013514
- Barker, C. H., Kourafalou, V. H., Beegle-Krause, C., Boufadel, M., Bourassa, M. A., Buschang, S. G., et al. (2020). Progress in operational modeling in support of oil spill response. *J. Mar. Sci. Eng.* 8. doi: 10.3390/jmse8090668
- Carvalho, S., Kürten, B., Krokos, G., Hoteit, I., and Ellis, J. (2019). “Chapter 3 - the red sea,” in *World seas: an environmental evaluation, 2nd ed.* Ed C. Sheppard (Academic Press), 49–74.
- Chiffings, A. W., Bleakley, C., Kelleher, G., and Wells, S. (1995). *Marine region 11 Arabian seas*. (World bank group) 3, 39–71.
- Crestaux, T., Le Maître, O., and Martinez, J.-M. (2009). Polynomial chaos expansion for sensitivity analysis. *Reliability Eng. System Saf.* 94, 1161–1172. doi: 10.1016/j.ress.2008.10.008
- Dasari, H. P., Desamsetti, S., Langodan, S., Attada, R., Kunchala, R. K., Viswanadhapalli, Y., et al. (2019). High-resolution assessment of solar energy resources over the arabian peninsula. *Appl. Energy* 248, 354–371. doi: 10.1016/j.apenergy.2019.04.105
- Debusschere, B., Sargsyan, K., Safta, C., and Chowdhary, K. (2017). *Uncertainty quantification toolkit (UQTk)* (Cham: Springer International Publishing), 1807–1827. doi: 10.1007/978-3-319-12385-1\_56
- De Dominicis, M., Pinardi, N., Zodiatis, G., and Archetti, R. (2013a). Medslik-ii, a lagrangian marine surface oil spill model for short-term forecasting – part 2: numerical simulations and validations. *Geoscientific Model. Dev.* 6, 1871–1888. doi: 10.5194/gmd-6-1871-2013
- De Dominicis, M., Pinardi, N., Zodiatis, G., and Lardner, R. (2013b). Medslik-ii, a lagrangian marine surface oil spill model for short-term forecasting – part 1: theory. *Geoscientific Model. Dev.* 6, 1851–1869. doi: 10.5194/gmd-6-1851-2013
- Dee, D. P., Uppala, S. M., Simmons, A. J., Berrisford, P., Poli, P., Kobayashi, S., et al. (2011). The era-interim reanalysis: configuration and performance of the data assimilation system. *Q. J. R. Meteorological Soc.* 137, 553–597. doi: 10.1002/qj.828
- Deguillard, E., Pannacci, N., Creton, B., and Rousseau, B. (2013). Interfacial tension in oil-water-surfactant systems: on the role of intra-molecular forces on interfacial tension values using DPD simulations. *J. Chem. Phys.* 138, 144102. doi: 10.1063/1.4799888
- Delvigne, G., and Sweeney, C. (1988). Natural dispersion of oil. *Oil Chem. pollut.* 4, 281–310. doi: 10.1016/S0269-8579(88)80003-0
- Dong, Y., Liu, Y., Hu, C., MacDonald, I. R., and Lu, Y. (2022). Chronic oiling in global oceans. *Science* 376, 1300–1304. doi: 10.1126/science.abm5940
- Duran, R., Nordam, T., Serra, M., and Barker, C. (2021). “Chapter 3 - horizontal transport in oil-spill modeling,” in *Marine hydrocarbon spill assessments*. Ed. O. Makarynskyy (Amsterdam, Netherlands: Elsevier), 59–96.
- Eldred, M. (2009). “Recent advances in non-intrusive polynomial chaos and stochastic collocation methods for uncertainty analysis and design,” in *50th AIAA/ASME/ASCE/AHS/ASC structures, structural dynamics, and materials conference* (Palm Springs, California, United States of America: AIAA). doi: 10.2514/6.2009-2274
- Fay, J. A. (1969). *The spread of oil slicks on a calm sea* (Boston, MA: Springer US), 53–63.
- Fernandez, M. (2010). *Wind coefficients and model calibration for drifter trajectories simulation with MOHID. tech. rep. WP2* (Lisbon, Portugal: AMPERA). Europe windCoefficient.
- Fingas, M. (1995). Water-in-oil emulsion formation: a review of physics and mathematical modelling. *Spill Sci. Technol. Bull.* 2, 55–59. doi: 10.1016/1353-2561(95)94483-Z
- Fingas, M., and Fieldhouse, B. (2014). *Water-in-Oil emulsions* Vol. 8 (Hoboken, New Jersey: John Wiley & Sons, Ltd), 225–270. doi: 10.1002/9781118989982.ch8
- Fogang, L. T., Kamal, M. S., Hussain, S. M. S., Kalam, S., and Patil, S. (2020). Oil/water interfacial tension in the presence of novel polyoxyethylene cationic gemini surfactants: impact of spacer length, unsaturation, and aromaticity. *Energy Fuels* 34, 5545–5552. doi: 10.1021/acs.energyfuels.0c00044
- French-McCay, D. P., Jayko, K., Li, Z., Spaulding, M. L., Crowley, D., Mendelsohn, D., et al. (2021). Oil fate and mass balance for the deepwater horizon oil spill. *Mar. pollut. Bull.* 171, 112681. doi: 10.1016/j.marpolbul.2021.112681
- Geary, E. (2017). *The API gravity of crude oil produced in the U.S. varies widely across states - today in energy - U.S* (USA: Energy Information Administration (EIA)).
- Ghanem, R. G., and Spanos, P. D. (1991). *Stochastic finite elements: a spectral approach* (New York, NY, USA: Springer New York).
- Goncalves, R. C., Iskandarani, M., Srinivasan, A., Thacker, W. C., Chassignet, E., and Knio, O. M. (2016). A framework to quantify uncertainty in simulations of oil transport in the ocean. *J. Geophysical Research: Oceans* 121, 2058–2077. doi: 10.1002/2015JC011311
- Hadigol, M., and Doostan, A. (2018). Least squares polynomial chaos expansion: a review of sampling strategies. *Comput. Methods Appl. Mechanics Eng.* 332, 382–407. doi: 10.1016/j.cma.2017.12.019
- Hodges, B. R., Orfila, A., Sayol, J. M., and Hou, X. (2015). “Operational oil spill modelling: from science to engineering applications in the presence of uncertainty,” in *Mathematical modelling and numerical simulation of oil pollution problems*. Ed. M. Ehrhardt (Cham: Springer International Publishing), 99–126.
- Hollebone, B. P. (2014). *Appendix a the oil properties data appendix* (Hoboken, New Jersey: John Wiley & Sons, Ltd), 575–681. doi: 10.1002/9781118989982.app1
- Homma, T., and Saltelli, A. (1996). Importance measures in global sensitivity analysis of nonlinear models. *Reliability Eng. System Saf.* 52, 1–17. doi: 10.1016/0951-8320(96)00002-6
- Hoteit, I., Abualnaja, Y., Afzal, S., Ait-El-Fquih, B., Akylas, T., Antony, C., et al. (2021). Towards an end-to-end analysis and prediction system for weather, climate, and marine applications in the red sea. *Bull. Am. Meteorological Soc.* 102, E99–E122. doi: 10.1175/BAMS-D-19-0005.1
- Huan, X., Safta, C., Sargsyan, K., Geraci, G., Eldred, M. S., Vane, Z. P., et al. (2018). Global sensitivity analysis and estimation of model error, toward uncertainty quantification in scramjet computations. *AIAA J.* 56, 1170–1184. doi: 10.2514/1.1056278
- Iskandarani, M., Le Hénaff, M., Thacker, W. C., Srinivasan, A., and Knio, O. M. (2016a). Quantifying uncertainty in gulf of mexico forecasts stemming from uncertain initial conditions. *J. Geophysical Research: Oceans* 121, 4819–4832. doi: 10.1002/2015JC011573
- Iskandarani, M., Wang, S., Srinivasan, A., Carlisle Thacker, W., Winokur, J., and Knio, O. M. (2016b). An overview of uncertainty quantification techniques with application to oceanic and oil-spill simulations. *J. Geophysical Research: Oceans* 121, 2789–2808. doi: 10.1002/2015JC011366
- Janeiro, J., Martins, F., and Relvas, P. (2012). Towards the development of an operational tool for oil spills management in the algarve coast. *J. Coast. Conserv.* 16, 449–460. doi: 10.1007/s11852-012-0201-8
- Kako, S., Isobe, A., Magome, S., Hinata, H., Seino, S., and Kojima, A. (2011). Establishment of numerical beach-litter hindcast/forecast models: an application to goto islands, japan. *Mar. pollut. Bull.* 62, 293–302. doi: 10.1016/j.marpolbul.2010.10.011
- Kampouris, K., Vervatis, V., Karagiorgos, J., and Sofianos, S. (2021). Oil spill model uncertainty quantification using an atmospheric ensemble. *Ocean Sci.* 17, 919–934. doi: 10.5194/os-17-919-2021
- KC, U., Aryal, J., Garg, S., and Hilton, J. (2021). Global sensitivity analysis for uncertainty quantification in fire spread models. *Environ. Model. Software* 143, 105110. doi: 10.1016/j.envsoft.2021.105110
- Keramea, P., Spanoudaki, K., Zodiatis, G., Gikas, G., and Sylaios, G. (2021). Oil spill modeling: a critical review on current trends, perspectives, and challenges. *J. Mar. Sci. Eng.* 9. doi: 10.3390/jmse9020181
- Khan, S., Al-Marhoun, M., Duffuaa, S., and Abu-Khamsin, S. (1987). “Viscosity correlations for saudi arabian crude oils,” in *All days* (Bahrain: SPE), 1–8.
- Kleinhaus, K., Woolstra, C. R., Meibom, A., Amitai, Y., Gildor, H., and Fine, M. (2020). A closing window of opportunity to save a unique marine ecosystem. *Front. Mar. Sci.* 7, 1117. doi: 10.3389/fmars.2020.615733
- Knio, O., and Le Maître, O. (2006). Uncertainty propagation in cfd using polynomial chaos decomposition. *Fluid Dynamics Res.* 38, 616–640. Recent Topics in Computational Fluid Dynamics. doi: 10.1016/j.fluiddyn.2005.12.003

- Kostianaia, E. A., Kostianoy, A., Lavrova, O. Y., and Soloviev, D. M. (2020). *Oil pollution in the northern red sea: a threat to the marine environment and tourism development* (Cham: Springer International Publishing), 329–362.
- Langodan, S., Cavaleri, L., Vishwanadhappalli, Y., Pomaro, A., Bertotti, L., and Hoteit, I. (2017). The climatology of the red sea – part 1: the wind. *Int. J. Climatology* 37, 4509–4517. doi: 10.1002/joc.5103
- Langodan, S., Cavaleri, L., Viswanadhappalli, Y., and Hoteit, I. (2014). The red sea: a natural laboratory for wind and wave modeling. *J. Phys. Oceanography* 44, 3139–3159. doi: 10.1175/JPO-D-13-0242.1
- Laurie, D. (1997). Calculation of gauss-kronrod quadrature rules. *Math. Comput.* 66, 1133–1145. doi: 10.1090/S0025-5718-97-00861-2
- Lehr, W., Jones, R., Evans, M., Simecek-Beatty, D., and Overstreet, R. (2002). Revisions of the ADIOS oil spill model. *Environ. Model. Software* 17, 189–197. doi: 10.1016/S1364-8152(01)00064-0
- Leitao, P., Malhadas, M., Ribeiro, J., Leitao, J., Pierini, J., and Otero, L. (2013). *An overview for simulating the blowout of oil spills with a three-dimensional model approach* (Caribbean Coast, Colombia: IST press), 97–115.
- Le Maître, O., and Knio, O. (2010). *Spectral methods for uncertainty quantification* (Netherlands: Springer Netherlands).
- Li, S. (2017). *Evaluation of new weathering algorithms for oil spill modeling* (Halifax, Canada: Dalhousie University). Master's thesis.
- Ling, K., and He, J. (2012). “A new correlation to calculate oil-water interfacial tension,” in *All days* (Kuwait City, Kuwait: SPE), 1–9.
- Lodise, J., Özgökmen, T., Griffa, A., and Berta, M. (2019). ). vertical structure of ocean surface currents under high winds from massive arrays of drifters. *Ocean Sci.* 15, 1627–1651. doi: 10.5194/os-15-1627-2019
- Lopes, I. E. (2016). *Uncertainty analysis in oil spill modelling – sensitivity and forcing analysis for a spill in the Portuguese coast and tagus estuary* (Lisbon, Portugal: Técnico Lisboa). Master's thesis.
- Lord, D., Allen, R., Rudeen, D., Wocken, C., and Aulich, T. (2018). DOE/DOT crude oil characterization research study, task 2 test report on evaluating crude oil sampling and analysis methods, revision 1 - winter sampling. doi: 10.2172/1458999
- Lütke, N., Panzeri, S., Brown, M., Broomhead, D. S., Knowles, J., Montemurro, M. A., et al. (2008). ). information-theoretic sensitivity analysis: a general method for credit assignment in complex networks. *J. R. Soc. Interface* 5, 223–235. doi: 10.1098/rsif.2007.1079
- Lüthen, M., Marelli, S., and Sudret, B. (2021). Sparse polynomial chaos expansions: literature survey and benchmark. *SIAM/ASA J. Uncertainty Quantification* 9, 593–649. doi: 10.1137/20M1315774
- Mackay, D., and Zagorski, W. (1981). “EnglishStudies of the formation of water-in-Oil emulsions,” in *Fourth Arctic marine oilspill program technical seminar*, vol. 75. (Environment Canada, Ottawa: Edmonton, Alberta).
- Mackay, D., and Zagorski, W. (1982). “EnglishWater-in-Oil emulsions: a stability hypothesis,” in *5th Arctic marine oilspill program technical seminar* (Environment Canada, Ottawa: Edmonton, Alberta), 61–74.
- Marelli, S., and Sudret, B. (2014). “Uqlab: a framework for uncertainty quantification in matlab,” in *Vulnerability, uncertainty, and risk* (University of Liverpool, United Kingdom: ASCE), 2554–2563. doi: 10.1061/9780784413609.257
- Marshall, J., Hill, C., Perelman, L., and Adcroft, A. (1997). Hydrostatic, quasi-hydrostatic, and nonhydrostatic ocean modeling. *J. Geophysical Research: Oceans* 102, 5733–5752. doi: 10.1029/96JC02776
- Martorell, S., Soares, C. G., and Barnett, J. (2008). *Safety, reliability and risk analysis* (London: CRC Press). doi: 10.1201/9781482266481
- Mateus, M. D., and Franz, G. (2015). Sensitivity analysis in a complex marine ecological model. *Water* 7, 2060–2081. doi: 10.3390/w7052060
- Maximenko, N., Hafner, J., and Niiler, P. (2012). Pathways of marine debris derived from trajectories of lagrangian drifters. *Mar. Pollut. Bull.* 65, 51–62. doi: 10.1016/j.marpolbul.2011.04.016
- Mishra, A. K., and Kumar, G. S. (2015). Weathering of oil spill: modeling and analysis. *Aquat. Proc.* 4, 435–442. doi: 10.1016/j.aapro.2015.02.058
- Mittal, H. V. R., Langodan, S., Zhan, P., Li, S., Knio, O., and Hoteit, I. (2021). Hazard assessment of oil spills along the main shipping lane in the red sea. *Sci. Rep.* 11, 17078. doi: 10.1038/s41598-021-96572-5
- Najm, H. N. (2009). Uncertainty quantification and polynomial chaos techniques in computational fluid dynamics. *Annu. Rev. Fluid Mechanics* 41, 35–52. doi: 10.1146/annurev.fluid.010908.165248
- Navarro Jimenez, M., Le Maître, O. P., and Knio, O. M. (2016). Global sensitivity analysis in stochastic simulators of uncertain reaction networks. *J. Chem. Phys.* 145, 244106. doi: 10.1063/1.4971797
- Neves, R. (1985). Biodimensional model for residual circulation in coastal zones: application to the sado estuary. *Annales geophysicae* (1983) 3, 465–471.
- Neves, R. (2013). The mohid concept, ocean modelling for coastal management—case studies with mohid. *MOHID's handbook* 1–11.
- Obuchi, T., and Kabashima, Y. (2016). Cross validation in LASSO and its acceleration. *J. Stat. Mechanics: Theory Experiment* 2016, 053304. doi: 10.1088/1742-5468/2016/05/053304
- Oliveira, A. R., Ramos, T. B., Simionesei, L., Pinto, L., and Neves, R. (2020). Sensitivity analysis of the mohid-land hydrological model: a case study of the ulla river basin. *Water* 12. doi: 10.3390/w12113258
- Olugbenga, A. G., Yahya, M. D., Garba, M. U., and Mohammed, A. (2020). Utilization of oil properties to develop a spreading rate regression model for nigerian crude oil. *Adv. Chem. Eng. Sci.* 10, 332–342. doi: 10.4236/aces.2020.104021
- Oudot, J., Merlin, F., and Pinvidic, P. (1998). Weathering rates of oil components in a bioremediation experiment in estuarine sediments. *Mar. Environ. Res.* 45, 113–125. doi: 10.1016/S0141-1136(97)00024-X
- Ranstam, J., and Cook, J. A. (2018). LASSO regression. *Br. J. Surg.* 105, 1348–1348. doi: 10.1002/bjs.10895
- Reed, M., Aamo, O. M., and Daling, P. S. (1995). Quantitative analysis of alternate oil spill response strategies using oscar. *Spill Sci. Technol. Bull.* 2, 67–74. doi: 10.1016/1353-2561(95)00020-5
- Reed, M., Johansen, Øistein, Brandvik, P. J., Daling, P., Lewis, A., Fiocco, R., et al. (1999). Oil spill modeling towards the close of the 20th century: overview of the state of the art. *Spill Sci. Technol. Bull.* 5, 3–16. doi: 10.1016/S1353-2561(98)00029-2
- Reed, M., Turner, C., and Odulo, A. (1994). The role of wind and emulsification in modelling oil spill and surface drifter trajectories. *Spill Sci. Technol. Bull.* 1, 143–157. doi: 10.1016/1353-2561(94)90022-1
- Rocha, L., Velho, L., and Carvalho, P. (2002). “Image moments-based structuring and tracking of objects,” in *Proceedings. XV Brazilian Symposium on Computer Graphics and Image Processing*, Fortaleza, Brazil. 99–105. doi: 10.1109/SIBGRA.2002.1167130
- Roth, V. (2004). The generalized lasso. *IEEE Trans. Neural Networks* 15, 16–28. doi: 10.1109/TNN.2003.809398
- Saltymakova, D., Desmond, D. S., Isleifson, D., Firoozy, N., Neusitzer, T. D., Xu, Z., et al. (2020). Effect of dissolution, evaporation, and photooxidation on crude oil chemical composition, dielectric properties and its radar signature in the arctic environment. *Mar. pollut. Bull.* 151, 110629. doi: 10.1016/j.marpolbul.2019.110629
- Sánchez-Minero, F., Sánchez-Reyna, G., Ancheyta, J., and Marroquin, G. (2014). Comparison of correlations based on api gravity for predicting viscosity of crude oils. *Fuel* 138, 193–199. doi: 10.1016/j.fuel.2014.08.022
- Schenk, C. J., Pollastro, R. M., and Hill, R. J. (2006). *Natural bitumen resources of the united states*. (Reston, VA, USA: USGS).
- Sobol, I. M. (1993). EnglishSensitivity estimates for nonlinear mathematical models. *Math. Model. Comput. Exper.* 1, 407–414.
- Sobol, I. (2001). Global sensitivity indices for nonlinear mathematical models and their monte carlo estimates. *Mathematics Comput. Simulation* 55, 271–280. doi: 10.1016/S0378-4754(00)00270-6
- Speight, J. (2020). “Chapter 9 - analysis of oil from tight formations,” in *Shale oil and gas production processes*. Ed. J. Speight (Cambridge MA, United States: Gulf Professional Publishing), 519–571.
- Sraj, I., Mandli, K. T., Knio, O. M., Dawson, C. N., and Hoteit, I. (2017). Quantifying uncertainties in fault slip distribution during the tōhoku tsunami using polynomial chaos. *Ocean Dynamics* 67, 1535–1551. doi: 10.1007/s10236-017-1105-9
- Srinivasan, A., LeHenaff, M., Kourafalou, V. H., Thacker, W. C., Tsinoremas, N. F., Helgers, J., et al. (2010). “Many task computing for modeling the fate of oil discharged from the deep water horizon well blowout,” in *2010 3rd workshop on many-task computing on grids and supercomputers* (New Orleans, LA, USA: IEEE), 1–7.
- Sudret, B. (2008). Global sensitivity analysis using polynomial chaos expansions. *Reliability Eng. System Saf.* 93, 964–979. doi: 10.1016/j.res.2007.04.002
- Thacker, W. C., Iskandarani, M., Gonçalves, R. C., Srinivasan, A., and Knio, O. M. (2015). Pragmatic aspects of uncertainty propagation: a conceptual review. *Ocean Model.* 95, 25–36. doi: 10.1016/j.ocemod.2015.09.001
- Tibshirani, R. (1996). Regression shrinkage and selection via the lasso. *J. R. Stat. Society. Ser. B (Methodological)* 58, 267–288.
- Transportation Research Board and National Research Council (2003). *Oil in the Sea III: inputs, fates, and effects* Vol. 4 (Washington, DC: The National Academies Press), 89–117. doi: 10.17226/10388
- van Sebille, E., Griffies, S. M., Abernathy, R., Adams, T. P., Berloff, P., Biastoch, A., et al. (2018). Lagrangian Ocean analysis: fundamentals and practices. *Ocean Model.* 121, 49–75. doi: 10.1016/j.ocemod.2017.11.008
- Viswanadhappalli, Y., Dasari, H. P., Langodan, S., Challa, V. S., and Hoteit, I. (2017). Climatic features of the red sea from a regional assimilative model. *Int. J. Climatology* 37, 2563–2581. doi: 10.1002/joc.4865
- Wang, S., Iskandarani, M., Srinivasan, A., Thacker, W. C., Winokur, J., and Knio, O. M. (2016). Propagation of uncertainty and sensitivity analysis in an integral oil-gas plume model. *J. Geophysical Research: Oceans* 121, 3488–3501. doi: 10.1002/2015JC011365
- Wang, S.-D., Shen, Y.-M., Guo, Y.-K., and Tang, J. (2008). Three-dimensional numerical simulation for transport of oil spills in seas. *Ocean Eng.* 35, 503–510. doi: 10.1016/j.oceaneng.2007.12.001
- Whitson, C. H., and R Brule, M. (2000). *EnglishPhase behavior (Society of petroleum engineers of AIME: Henry I. doherty memorial fund of AIME, society of petroleum engineers)*. (Pennsylvania, USA: Society of Petroleum Engineers).
- Wiener, N. (1938). The homogeneous chaos. *Am. J. Mathematics* 60, 897–936. doi: 10.2307/2371268

Winokur, J., Conrad, P., Sraj, I., Knio, O., Srinivasan, A., Thacker, W. C., et al. (2013). *A priori* testing of sparse adaptive polynomial chaos expansions using an ocean general circulation model database. *Comput. Geosciences* 17, 899–911. doi: 10.1007/s10596-013-9361-3

Winoto, W., Loahardjo, N., Takamura, K., and Morrow, N. R. (2014). Spreading and retraction of spilled crude oil on seawater. *Int. Oil Spill Conf. Proc.* 2014, 1465–1473. doi: 10.7901/2169-3358-2014.1.1465

Xu, H.-L., Chen, J.-N., Wang, S.-D., and Liu, Y. (2012). Oil spill forecast model based on uncertainty analysis: a case study of Dalian oil spill. *Ocean Eng.* 54, 206–212. doi: 10.1016/j.oceaneng.2012.07.019

Yao, F., Hoteit, I., Pratt, L. J., Bower, A. S., Köhl, A., Gopalakrishnan, G., et al. (2014a). Seasonal overturning circulation in the red sea: 2. winter circulation. *J. Geophysical Research: Oceans* 119, 2263–2289. doi: 10.1002/2013JC009004

Yao, F., Hoteit, I., Pratt, L. J., Bower, A. S., Zhai, P., Köhl, A., et al. (2014b). Seasonal overturning circulation in the red sea: 1. model validation and summer circulation. *J. Geophysical Research: Oceans* 119, 2238–2262. doi: 10.1002/2013JC009331

Zhan, P., Krokos, G., Guo, D., and Hoteit, I. (2019). Three-dimensional signature of the red sea eddies and eddy-induced transport. *Geophysical Res. Lett.* 46, 2167–2177. doi: 10.1029/2018GL081387

Zhan, P., Subramanian, A. C., Yao, F., Kartadikaria, A. R., Guo, D., and Hoteit, I. (2016). The eddy kinetic energy budget in the red sea. *J. Geophysical Research: Oceans* 121, 4732–4747. doi: 10.1002/2015JC011589

Zodiatis, G., Lardner, R., Spanoudaki, K., Sofianos, S., Radhakrishnan, H., Coppini, G., et al. (2021). “Chapter 5 - operational oil spill modelling assessments,” in *Marine hydrocarbon spill assessments*. Ed. O. Makarynskyy (Amsterdam, Netherlands: Elsevier), 145–197.